Two-Dimensional reactive transport modeling of CO2 injection in a saline aquifer at the Sleipner site, North sea

Pascal Audigane, Irina Gaus, Isabelle Czernichowski-Lauriol, Karsten Pruess, Tianfu Xu

TWO-DIMENSIONAL REACTIVE TRANSPORT MODELING OF CO_2 INJECTION IN A SALINE AQUIFER AT THE SLEIPNER SITE

PASCAL AUDIGANE [1], IRINA GAUS [1], ISABELLE CZERNICHOWSKI-LAURIOL[1], KARSTEN PRUESS [2], TIANFU XU [2]

(1) BRGM, French Geological Survey, 3 Av. Claude Guillemin, BP 6009 45060 ORLEANS Cedex 2, FRANCE

(2) LBNL, Lawrence Berkeley National Laboratory, Earth Sciences Division, University of California, One Cyclotron Road, Berkeley, CA 94720, USA

ABSTRACT. This paper presents a 2D reactive transport model of long-term geological storage of carbon dioxide. A data set from the Utsira formation in Sleipner (North Sea) is utilized for geochemical simulation, while the aquifer is approximated as a 2D cylindrically symmetric system. Using the reactive transport code TOUGHREACT, a 25 year injection scenario followed by a 10 000 year storage period are simulated. Supercritical CO_2 migration, dissolution of the CO_2 in the brine, and geochemical reactions with the host rock are considered in the model. Two mineralogical assemblages are considered in the Utsira formation, a sand formation that is highly permeable and a shale formation representing four semi-permeable layers in the system that reduce the upward migration of the supercritical CO_2. The impacts of mineral dissolution and precipitation on porosity are calculated. Furthermore, the 2D cylindrical geometry of the mesh allows simulating both the upward migration of the supercritical gas bubble as well as the downward migration of the brine containing dissolved CO_2. A mass balance of the CO_2 stored in, respectively, the supercritical phase, dissolved in the aqueous phase, and sequestered in solid mineral phases (carbonate precipitation) is calculated over time. Simulations with a lower residual gas

saturation and with different mesh refinement are also performed to test the sensitivity on mass balance estimates.

INTRODUCTION

Geological storage of carbon dioxide is considered one of the most efficient means for a rapid reduction of greenhouse gas emissions into the atmosphere (Holloway, 1997, Holloway, 2002 and IPCC, 2002). Three types of geologic systems are under consideration for CO_2 storage in the subsurface (Holloway, 1997), (i) depleted oil or gas reservoirs, (ii) unmineable coal beds and (iii) saline aquifers. Deep saline aquifers offer the advantages of having more volume capacity and being the more abundant in the subsurface compared to the other systems.

CO_2 is expected to be injected as a dense phase under supercritical conditions in order to occupy less volume into the underground. In the following, the term "gas" will be used to denote carbon dioxide under supercritical conditions, which forms a phase separate from the aqueous or liquid phase (brine). Three processes of CO_2 trapping can be distinguished (Hitchon, 1997): (i) *structural trapping,* in which CO_2 is trapped as a dense phase according to the structural lithology of the storage zone, (ii) *dissolution trapping,* which represents CO_2 dissolved in the liquid phase (oil or brine), and (iii) *mineral trapping,* representing CO_2 that has been incorporated into minerals due to chemical precipitation. To ensure safety, a low permeable formation, called the *cap rock*, is required on the top of the storage zone to prevent the upward migration of the supercritical CO_2. On the other hand, a storage zone with a high porosity will be preferable in order to provide a larger volume capacity. In order to maintain the CO_2 in a supercritical state, injection should be performed at depths greater than 800 m (Holloway, 1997). Residence times of CO_2 in the gas phase can be several thousand years before complete dissolution (Lindeberg and Bergmo, 2002). The brine containing the dissolved CO_2 is slightly denser than the original brine, inducing gravity-driven flow and convective fluid circulation (Weir and others, 1996). This will promote mixing of fluid, mainly controlled by the vertical

permeability, which is favorable for CO_2 dissolution (Lindeberg and Bergmo, 2002). Mineral trapping offers a larger sequestration potential with residence times on the order of geologic times (Bachu and others, 1994). Experiments have been conducted to assess the potential of mineral trapping in different geological systems (Gunter and others, 1997, Rochelle and others, 2002). Natural carbon dioxide accumulations can be used as analogues for studying CO_2 impact on the host rocks after long residence times (Pearce and others, 1996, Forster and others, 2004). Nevertheless, the initial mineral assemblage controlling CO_2 mineral sequestration is difficult to characterize. Numerical modeling offers a means of providing short and long-term storage predictions, and aids in monitoring of CO_2 migration during and after injection.

Long-term balance estimates of the three trapping mechanisms previously described require the development of a reactive transport model that is able to accurately describe hydrodynamic and geochemical processes. Due to computational constraints, models typically will focus either on a detailed description of geochemical processes (complex mineral assemblage with kinetic precipitation and dissolution) while simplifying fluid flow (one dimensional with constant velocity), or will emphasize detailed fluid flow simulation (2D or 3D heterogeneous model with gravity effects on the supercritical and dissolved carbon dioxide) while employing a simplified description of geochemical reactivity (simplified mineralogical assemblage, no kinetics).

The objective of this paper is to develop a model of carbon dioxide injection into a saline formation that includes a detailed mineralogical description of the storage formation, a good representation of the gas and liquid-phase flow in the aquifer, and a realistic geologic model for the reservoir containing alternating sand and clay layers. Using a conceptual model based on the Sleipner dataset, different realistic mineralogies are implemented for the sand and shale layers, and a 2D vertical model is built with a radial mesh geometry containing 22 layers, including 4 semi-permeable shale layers. This provides a good description of the horizontal and vertical migration of the gas bubble, and of the chemical reactivity associated with the dissolved CO_2.

Simulations are performed with the code TOUGHREACT (Xu and others, 2006) for a long storage period (10 000 years). The geochemical impacts from the interplay between flow and geochemical reactions are evaluated, and a total mass balance of storage capacity is established for the three different trapping mechanisms for a time period of 10 000 years. Impacts on formation porosity are evaluated, and a sensitivity analysis on different physical parameters and on grid refinement is discussed. It is not our intent to provide a detailed sensitivity analysis on the selection of minerals, nor on their specific parameters (rates, specific surface areas). It is our view that such analysis should be performed using batch models or simple flow models, rather than complex coupled models as presented here.

STATE OF THE ART

Recent numerical modeling of CO_2 sequestration can be classified into three different categories, (i) hydrodynamic modeling, corresponding to the simulation of both structural and dissolution trapping, (ii) geochemical modeling, corresponding to the characterization of mineral trapping only, and (iii) reactive transport modeling, corresponding to simulations that couple structural, dissolution and mineral trapping processes. For each of these categories, a different subset of physical and chemical processes is modeled.

Hydrodynamic modeling

Many hydrodynamic simulations of CO_2 injection can be found in the literature. Lindeberg and others (2000) and Lindeberg and Bergmo (2002) have provided simulations for the upward migration of the CO_2 bubble in the Utsira formation for the Sleipner project. For their study, simulations were performed with the black oil simulator ECLIPSE that is commonly used in petroleum engineering. No geochemical reactions were considered in the model. Convective fluxes of the brines containing dissolved CO_2 were observed in long term simulations (Lindeberg and Bergmo, 2002). The model was calibrated according to several seismic surveys that provided

estimates of the volume occupied by the supercritical carbon dioxide in the aquifer (Lindeberg and others, 1999, Torp and Gale, 2002). Another simulation using ECLIPSE was performed for the Weyburn project (Zhou and others, 2004). In this case, CO_2 is injected partially with the objective to enhance oil recovery. An oil phase is considered in the simulations, but geochemical reactivity is not calculated.

Much work has been published using the TOUGH family of codes (Pruess, 1987, 1991, 2004). TOUGH2 was originally developed for geothermal reservoir engineering, nuclear waste disposal studies, groundwater remediation, and unsaturated and saturated-zone hydrology. The adaptation of this multiphase fluid and heat flow simulator to geologic storage of CO_2 allows simulations of carbon dioxide injection into deep saline aquifers, as well as fluid migration along fault zones, and CO2 injection into natural gas reservoirs for combining storage with enhanced gas production (Weir and others, 1996, Pruess and Garcia, 2002, Oldenburg and Benson, 2002). A code intercomparison study using different test problems associated with CO_2 injection allowed to evaluate discrepancies between different simulators (Pruess and others, 2004).

Batch geochemical modeling

Batch geochemical modeling allows to identify the main chemical reactions in the formation, based on a given mineral assemblage and the initial speciation of the aqueous phase enriched in dissolved CO_2. The kinetics of mineral dissolution and precipitation plays a major role. Gaus and others (2004) have developed a long-term batch geochemical study of two natural CO_2 analogues at Montmiral (France) and Messokampos (Greece). Using the PHREEQC code developed by the USGS (Parkhurst and Appelo, 1999), simulations were performed in order to assess long-term mineral trapping and porosity changes due to the presence of CO_2. Pruess and others (2001) and Xu and others (2004) have presented long-term batch geochemical modeling of mineral trapping in deep aquifers through carbonate mineral precipitation. Their simulations were carried out using TOUGHREACT, which is an enhancement of the multi-phase fluid and

heat flow code TOUGH2 to reactive transport (Xu and Pruess, 2001). More details on TOUGHREACT will be provided later in this paper as it is the code used in the present study.

Reactive transport modeling

Batch geochemical modeling is of limited utility for CO_2 storage capacity estimates, because hydrodynamics may play an important role in the sequestration process. Coupling hydrodynamics with geochemical reactions can increase the accuracy of predictions. Gaus and others (2005) have developed a one-dimensional reactive transport model of CO_2 diffusion through the cap rock at Sleipner using PHREEQC. Diffusion of CO_2 through the rock is modeled by Henry's law with a constant fugacity coefficient. Using TOUGHREACT, Xu and others (2005) presented a 1D vertical reactive transport model of CO_2 geologic storage for a sandstone-shale system with a very detailed mineralogical assemblage that is representative of Texas Gulf Coast sediments. CO_2 dissolution is calculated with an enhanced Henry's law that includes effects of temperature, pressure and salinity (Pruess and García, 2002). Another 1D horizontal model has been developed for CO_2 injection in deep arenaceous formations of U.S. Gulf Coast (Xu and others, 2003). In this case, the mesh geometry is radial and hence does not consider non-uniform sweep that may occur due to formation heterogeneities, or due to buoyancy forces that may drive supercritical CO_2 to the top of the formation and dissolved CO_2 to the bottom. A very complete mineral assemblage typical of Gulf Coast formations was selected, and porosity changes were calculated for residence times of up to 10 000 years. Lagneau and others (2005) proposed a 2D horizontal model for CO_2 injection into two deep saline aquifers, the Dogger (Paris Basin) and the sandstone aquifer of the Bunter (North Sea). The HYTEC code used in their study does not consider two-phase flow and therefore only the dissolved part of the injected carbon dioxide is considered. Johnson and others (2001) performed simulations for a period of 20 years with 10 years of CO_2 injection in a Sleipner-like case. Three 2D vertical conceptual reservoir models were proposed for the Utsira formation, differing in the presence of intra-

aquifer shales. For their simulations, a software package based on NUFT for the reactive transport part, and SUPCRT92 and GEMBOCHS for the geochemical and thermodynamics/kinetic databases, was used (Nitao, 1998; Johnson and others, 1992; Shock, 1998, Johnson and Lundeen, 1994). No convective flows due to density differences were considered in the model, and dependence of CO_2 dissolution on pressure or temperature was not accounted for. A 2D vertical reactive transport model of CO_2 injection in saline reservoirs of the Colorado Plateau was developed that considers time periods of up to 100 000 years with two different meshes, using CHEMTOUGH which is another adaptation of TOUGH2 to reactive transport modeling (White and others, 2001, 2005). CHEMTOUGH includes an implicit scheme for the coupling between hydrodynamics and geochemistry (White, 1995), while TOUGHREACT uses a sequential iteration approach (Yeh and Tripathi, 1991). A finely gridded simulation of White and coworkers present a very detailed model of the hydrology of the Colorado plateau, but without considering geochemical reactions. A coarser mesh was used for a reactive transport simulation of CO_2 injection that includes a complete mineralogy with plagioclase, K-feldspar, dolomite, quartz, mixed clays, illite, iron minerals and calcite. However, the complex mineralogy of the different layers did not allow for a detailed interpretation.

Nghiem and others (2004), presented a study including 1D, 2D and even 3D models of CO_2 injection in aquifers using the commercial GEM-GHG code that is capable of modeling convective and dispersive flows, as well as calculating phase equilibrium for reactions between the oil, gas and aqueous phases, and chemical equilibrium or kinetic dissolution and precipitation reactions between minerals. A method for solving all equations simultaneously in a more robust way is described. A simpler set of reactions was chosen for the 3D models than for the 1D or 2D model. Frangeul and others (2004) have presented a simulation of CO_2 injection at Sleipner using GEM-GHG. The simulation for a time period of up to 5000 years included 3D convective flows induced by density included 3D convective flows induced by density differences, but used

homogeneous reservoir properties and a very simplified mineral assemblage containing only calcite and dolomite.

THE SLEIPNER SITE

The CO_2 injection at Sleipner

The Sleipner West natural gas field is located in the centre of the North Sea (Norwegian block 15/9). The gas is produced via several wells and transported to a process and treatment platform in order to reduce its CO_2 content of 1 million tons annually (fig. 1). Rather than venting the CO_2 to the atmosphere, and because of economic incentives (a Norwegian tax of 55 $ per ton of CO_2 emitted), a decision was taken by the field operator Statoil and other partners to inject the carbon dioxide underground into the Utsira formation, located above the gas reservoir. This demonstration project started in 1996 and EU funded research started in 1998 (SACS2, 2002).

The Utsira formation is a large sandy aquifer extending over 26100 km² located at a depth from 700 to 1000 m. Four seismic surveys have been conducted since the start of injection in 1996 at a rate of one million tons per year. Visualizations of the gas bubble evolution have been produced before and after injection in 1999, 2001 and 2002 (Torp and Gale, 2002, IEAGHG, 2005). The upward migration of the supercritical CO_2 due to buoyancy effects amounts to about 250 m after three years, with a lateral extension of about 600 m, and seems to have been stopped by the cap rock situated at the top of the formation (Arts and others, 2004). The seismic profiles have revealed the presence of CO_2 accumulations in a layered structure, attributed to the presence of low-permeable layers that determine the vertical and lateral extent of the CO_2 plume in the aquifer. A reservoir modeling study has reproduced plume contours determined from seismic monitoring after three years of injection, using multiphase flow simulators without considering chemical reactivity (Lindeberg and others, 2000, SACS2, 2002). In this modeling work, the presence of low-permeable layers was necessary to fit the seismic profiles. Therefore,

in this paper we will model the Utsira formation as an assemblage of two lithologies, one called "sand" for the highly permeable part of the porous media and one called "shale" for the low-permeable layers.

Mineral composition of the Utsira formation

The mineral composition of both the shales and the sands was specified in such a way that their composition is realistic without taking into account large amounts of different clay minerals, or minerals that are present only in tiny amounts. This would needlessly complicate the dissolution and precipitation patterns resulting from the coupled 2D model and would not allow for a convincing interpretation of the geochemical interactions and of the identification of the driving reaction mechanisms. We also neglect solid solutions, such as plagioclase (Gaus and others, 2005), and do not consider interactions with organic matter. The latter would induce redox reactions that are of minor significance here, yet would greatly increase the computational work (Xu and others, 2005).

Sand.--- The "sand" part of the Utsira formation sandstone comprises a poorly cemented, fine-to-medium grained, moderately sorted sand. It is composed predominantly of subangular to subrounded, occasionally angular, quartz grains with minor k-feldspar, plagioclase, calcite and coarse to gravel-sized shell fragments, including siliceous sponge spicules, foraminifera and radiolarian tests. Rare biotic flakes and rare glauconitic grains are present; also clay grade materials are rare. The mineralogical composition of the Utsira Formation between 1085 and 1086 m depth has been used as a reference (Table 1). It consists mainly of quartz, k-feldspar, plagioclase, mica and calcite. Minor constituents are chlorite, zeolite, Ti-oxides, ilmenite and pyrite.

Chlorite (an iron-rich variant) is used as a representative for the chlorite group. Plagioclase is modeled as pure albite since this phase is more stable than anorthite, which forms the other end member of the plagioclase solid solution series in sedimentary rocks. Furthermore, no exact

plagioclase composition is available from mineralogical analysis. The phase described as mica is considered as muscovite, one of the most common micas. Chalcedony is selected instead of quartz since chalcedony is generally the controlling SiO_2-phase in sedimentary rocks at low temperatures (Appelo and Postma, 1993). The very small zeolite fraction is not modeled because its exact composition is not known and therefore its thermodynamic properties are extremely uncertain. Also, the trace minerals apatite, ilmenite, pyrite, and Ti-oxides are not included in the model.

Chalcedony and kaolinite are commonly observed to precipitate under diagenetic circumstances (Bjørlykke and others, 1992). The same holds for carbonate minerals such as calcite, siderite and disordered dolomite. These minerals are therefore potential reaction products of interaction with CO_2 and are included as secondary minerals.

Including dawsonite in the secondary mineral selection needs some justification. Dawsonite is a rare mineral that is assumed to form when aluminiferous minerals are subjected to highly alkaline solutions which contain increased quantities of sodium carbonates and bicarbonates (Stankevitch and Batalin, 1976). Dawsonite has been observed in natural CO_2 reservoirs such as the Bowen-Gunnedah-Sydney basin in Australia (Baker and others, 1995) and beneath the Colorado Plateau and Southern Rocky Mountains (Moore and others, 2003). Since dawsonite is also supersaturated when combining high CO_2 concentrations with the cap rock mineralogy it was decided to include it in the secondary mineral assemblage.

Shale.--- As there is no available data to characterize the "shale" part of the Utsira formation we will assume in this study that shale mineralogy is equivalent to the cap rock mineralogy as described by Gaus and others (2005). This mineralogical composition was based on the study of drill cuttings taken at the base of the cap rock revealing presence of quartz, undifferentiated mica, kaolinite, k-feldspar, calcite, smectite, albite, chlorite, siderite and pyrite (Bøe and Zweigel, 2001, Kemp and others, 2002). In the present study, mica is represented by muscovite and quartz by chalcedony. Smectite was not considered in the model as the

geochemical equilibration between all the cap rock minerals and the formation water could not be obtained, meaning that one mineral phase at least disappeared during the initial speciation (Table 2). Furthermore, the exact mineralogical composition of the smectite is not specified in the analysis and can vary significantly, while the molar volume is poorly described in the literature. More details are provided in section 4.1.2. on initial equilibration with mineralogy and formation water.

Formation water

Although no samples from the Utsira reservoir at Sleipner are available, several samples were taken at nearby locations such as Oseberg. A homogeneous porewater composition throughout the Utsira formation at Sleipner can reasonably be assumed. The composition selected for our model is similar to the Synthetic Utsira Porewater (SUP) that was used for laboratory experiments performed with Utsira sands (Czernichowski-Lauriol and others, 1996, 2002; Rochelle and Moore, 2002).

This composition is taken as a starting point and is subsequently equilibrated, by means of geochemical modeling, with muscovite, albite, chalcedony, k-feldspar and chlorite, resulting in aqueous concentrations as given in Table 3.

NUMERICAL METHOD

Computer program

All simulations have been performed using the non-isothermal program TOUGHREACT (Xu and Pruess, 2001; Xu and others, 2006). This code was developed by introducing reactive geochemical transport into the existing multi-phase fluid and heat flow code TOUGH2 V2 (Pruess and others, 1999). A specific Equation Of State (EOS) fluid property module has been developed for multiphase flow dynamics for CO_2 disposal into saline aquifers, considering the three active phases water-salt-CO_2 (Pruess and García, 2002). An accurate description of the

thermo-physical properties (density, viscosity, enthalpy and fugacity) of mixtures of brines and CO_2 is provided.

The numerical method for fluid flow simulations is based on the integral finite difference method for space-discretization (Narasimhan and Witherspoon, 1976). An implicit time-weighting scheme is used for the flow and transport equations. A sequential iterative approach is used for the coupling between transport and geochemical reactions (Yeh and Tripathi, 1991). Variably saline water and supercritical CO_2 are considered as mobile phases.

The system of equations generated by the chemical reactions is solved using a Newton-Raphson iterative method (Xu and Pruess, 2001). Any number of species present in the liquid, gas and solid phase can be considered. Distribution of aqueous species is controlled by local equilibrium. Activity coefficients for aqueous species are calculated from the extended Debye-Hückel equation (Helgeson and Kirkham, 1974). The treatment of dissolution of CO_2 in the brine is presented in Section 3.2. Mineral dissolution/precipitation can proceed subject either to local equilibrium or to kinetic conditions. The kinetic rate law used is presented in Section 3.3.

Dissolution of CO_2

During dissolution of CO_2 in the brine, gaseous and aqueous CO_2 are assumed to be in equilibrium, hence:

$$CO_{2(sc)} \rightleftarrows CO_{2(aq)} \tag{1}$$

where subscripts "sc" and "aq" denote supercritical and aqueous CO_2, respectively. In the TOUGHREACT code, solubility of CO_2 in brine is represented by an extended version of Henry's law allowing for salinity effects ("salting out") as well as for fugacity corrections to CO_2 partial pressure (Pruess and García, 2002):

$$K\Gamma P = \gamma C \tag{2}$$

Where K is the equilibrium constant depending on the temperature T (Xu and others, 2004), P is the partial pressure (bar), γ is the aqueous CO_2 activity coefficient, C is the aqueous concentration (mol/kg H_2O) and Γ is a fugacity parameter depending on pressure and temperature according to Spycher and Reed (1988).

Kinetics of mineral dissolution and precipitation

A general kinetic rate law for mineral dissolution and precipitation is used (Lasaga, 1984, Steefel and Lasaga, 1994):

$$r_m = k(T)_m A_m \left[1 - \left(\frac{Q_m}{K_m}\right)\right] \tag{3}$$

where m is the mineral index, r_m is the dissolution/precipitation rate (positive values indicates dissolution), A_m is the specific reactive surface area per kg of water, $k(T)_m$ is the temperature-dependent rate constant, K_m is the equilibrium constant for the mineral water reaction written for the destruction of one mole of mineral, and Q_m is the corresponding ion activity product. For all minerals the same rate law is used for precipitation and dissolution.

The temperature dependence of the reaction rate constant is expressed via an Arrhenius equation (Lasaga, 1984, Steefel and Lasaga, 1994):

$$k = k_{25}\left[\frac{-E_a}{R}\left(\frac{1}{T} - \frac{1}{298.15}\right)\right] \tag{4}$$

where E_a is the activation energy, k_{25} is the rate constant at 25 °C, R is the gas constant, and T is absolute temperature.

Table 4 provides the parameters and the references for the kinetics of dissolution and precipitation of all minerals used in the simulations. Some kinetic parameters are taken directly from the referenced scientific literature and others are set to minerals with known kinetic properties. Specific reactive surface area remains difficult to characterize. The values used in this study correspond to those used by Xu and others (2005) and were originally taken from

Sonnenthal and Spycher (2001). These values are calculated assuming a rock framework composed of a cubic array of truncated spheres. Surface areas were increased for clay minerals kaolinite and illite to account for edges in these sheet silicate minerals. More details on the choice of the kinetic parameters for mineral reaction rates and sensitivity analysis on these parameters are discussed in Xu and others (2005).

SIMULATION RESULTS

In this section, results from batch geochemical modeling and 2D reactive transport modeling are presented. Batch geochemical modeling does not consider any fluid flow in the studied area but allows defining the most important geochemical reactions involved in the sequestration process.

Batch geochemical modeling

Modeling scenario.--- Batch geochemical modeling is performed first to simulate the geochemical impact of CO_2 on the two chosen mineral assemblages. For the sand formation, the simulations are performed for a space domain corresponding to a grid cell with a 2 km x 2 km area and a thickness of 184 m (Fig. 2). This volume is an estimate of the global volume occupied by the gas bubble and the carbon dioxide dissolved after 10,000 years. Considering a porosity of 42 % and temperature and pressure conditions of (T, P) = (37°C, 100 bar), the initial amount of supercritical CO_2 is fixed at a gas saturation of 0.11. This value corresponds to a mass of supercritical CO_2 of 2.36 10^{10} kg, as would be injected over a 25 year period at a rate of 30 kg/s. For the shale case, simulations are conducted with the same gas saturation in order to keep the same reactivity as in the sand, but with a lower porosity value of 10.25 %

The simulation is conducted for a storage period of 10,000 years. Temperature logs revealed a rather small variation of 5 C° from top to bottom (Eric Lindeberg, private communication). Therefore, no heat exchange is considered in this work and the temperature is

held constant at 37 °C. Initial reservoir pressure is 100 bars which corresponds approximately to initial pressure at the injection depth. Temporal modification of porosity and permeability can be considered in TOUGHREACT (Xu and others, 2003). Changes of porosity are calculated from mineral volume changes due to chemical dissolution or precipitation. Changes of permeability from porosity change will not be considered in this study, because the impact on permeability is rather small, while the computational penalty is substantial when exercising this option (Xu and others, 2003).

In the following we present results from batch simulation studies (no flow) for the "sand" and "shale" formations, respectively. These provide a preliminary outlook on long-term geochemical impacts and the different trapping mechanisms of CO_2 storage.

Batch simulation results

First, a batch geochemical simulation is performed without considering the presence of CO_2 in the domain to assess the reactivity of initial water with minerals. Then, a batch model containing CO_2 is presented.

Background without CO_2 injection for the shale and the sand system.--- In the shale batch model we obtain a slight porosity decrease of the order of $0.5\ 10^{-5}$. This change is induced by a slight dissolution of muscovite and chalcedony resulting in minor precipitation of kaolinite and k-feldspar (about 2 moles per m^3 of medium over 10 000 years; see Fig. 3). This reactivity is minor and negligible compared to reactivity and porosity changes from interactions with CO_2 over the same time period (see below). In the sand batch simulation no significant reactivities are observed.

Batch reactions with CO_2 injection in the Shale.--- Figures 4 and 5 present the evolution of pH, porosity, and aqueous, gaseous and mineral species during the batch simulations of CO_2 reacting with the shale and sand formations. For short term reactions only, an initial pH decrease occurs, immediately following contact of the formation water with CO_2, which triggers

dissolution of carbonates, stabilizing pH at a value of 5.13. The amount of carbonates dissolved is minor, however, when compared to the amount of minerals precipitated over long time periods. For long term reactions, alumino-silicates dominate the geochemical interactions. There are three major reactions (a – c):

The alteration of chlorite consuming calcite and resulting in the trapping of CO_2:

$$Fe_{2.5}Mg_{2.5}Al_2Si_3O_{10}(OH)_8 + 2.5\ CaCO_3 + 5\ CO_2$$

Chlorite calcite

$$\rightarrow 2.5\ FeCO_3 + 2.5\ MgCa(CO_3)_2 + Al_2Si_2O_5(OH)_4 + SiO_2 + 2H_2O$$

siderite dolomite kaolinite chalcedony (a)

Both Fe and Mg act as donor cations for the trapping of CO_2 in the form of siderite and dolomite. Kaolinite is also formed but provides no trapping capacity for CO_2. The total mole transfer in this reaction is of the order of 34 moles of chlorite per m^3 medium (170 moles of CO_2).

The second CO_2 trapping reaction is the alteration of albite, leading to the formation of dawsonite and chalcedony:

$$NaAl_3Si_3O_8 + CO_2 + H_2O \rightarrow NaAlCO_3(OH)_2 + 3\ SiO_2$$

albite dawsonite chalcedony (b)

This reaction occurs faster than the previous reaction and results in the dissolution of 120 moles of albite over 10 000 years.

Both reactions result in a significant amount of SiO_2 coming into solution which lead to precipitation of chalcedony. Chalcedony may not form in reality, but the increased SiO_2 concentration can act as a driver for the following reaction:

$$KAl_3Si_3O_{10}(OH)_2 + 2\ SIO_2 + H_2O \rightarrow KAlSi_3O_8 + Al_2Si_2O_5(OH)_4$$

muscovite chalcedony k-feldspar kaolinite (c)

This reaction, indirectly driven by the presence of CO_2, causes a significant mole transfer (192 moles of muscovite react over 10 000 years) and also has an impact on porosity.

After approximately 2600 years all CO_2 present in the cell has been consumed in reactions and this causes the pH to increase to a value slightly above 6.5. At this point, in terms of volume of minerals, 0.3 % of the albite and 0.7 % of the chlorite initially present has reacted. Once the CO_2 is consumed and due to the pH increase, part of the chlorite re-precipitates. Dissolution of albite continues, although at a slower rate.

The overall reactivity results in an absolute porosity reduction of approximately 0.01 (from 10.25 % initially down to 9.3 % after 10 000 years) or a relative porosity reduction of 9 % in this closed system.

Batch reactions with CO_2 injection in the Sand.--- In the case of the *sand*, the reactivity is slightly different, which can be attributed mainly to the larger porosity that allows for a stronger interaction with the dissolved species. Chlorite alteration causes the transformation of 25 moles of chlorite, while albite alteration transforms 14 moles of albite, reacting with a total of 138 moles of CO_2. In this case the alteration of albite is more limited than for the shales. A total amount of 120 moles of dawsonite is formed, of which 116 moles result from the reaction of the Na present in the brine:

$$2\,Na^+ + Al_2Si_2O_5(OH)_4 + 2CO_2 + 3OH^- \rightarrow 2\,NaAlCO_3(OH)_2 + 2\,SiO_2 + H$$

kaolinite dawsonite chalcedony (d)

The combination of both reactions transfers less SiO_2 into solution compared to reactions a-b for the clays. The alteration of muscovite to k-feldspar, which requires a large SiO_2 source, is limited to a total transfer of 50 moles.

Because the amount of CO_2 present is larger for the sand due to its larger porosity, within 10,000 years only a fraction of the CO_2 is consumed in reactions (resulting in a concentration decrease from initial 1.16 mole/kg to 0.88 mole/kg). After 10,000 years, only 0.002 % of the albite and 0.0002 % of the chlorite has reacted. The CO_2-induced reactions also cause a slight decrease in porosity, from initial 40 % to 39.6 % or a relative decrease of 1%.

2D reactive transport modeling

Geometric configuration.--- In this paper, the Utsira formation geometry is approximated by a vertical 2D mesh with a cylindrical geometrical configuration, centered around an injection point located 155 m beneath the top of the 184 m thick formation (Fig. 6A). The porous media form a layered structure, composed from top to bottom of four sand layers of 25 m thickness that are separated by shale layers of 5 m thickness and a bottom sand layer of 70 m thickness into which the CO_2 is injected. The mesh contains 22 layers in the vertical and 52 cells in the radial direction. The first cell has a radius of 10 m, and is followed by 20 cells with radial increments increasing in logarithmic progression out to 1 km. Beyond this are 15 cells with another logarithmic progression to 1 km. Beyond 1 km are 20 more increments with logarithmic progression to a radial distance of 3 km, and then 5 grid cells extending out to 100 km from the injection point, so that the model system would be infinite acting.

Because of computing time constraints, a 3D model was not considered in this study. Pruess and others (2004) represented the Sleipner system as a 2D vertical section perpendicular to the horizontal injection well which has a screen length of 100 m. Lindeberg and others (2000) in a first approach used a radial model consisting of a 160 m tall cylinder with a diameter of 1600 m. Seismic surveys show an approximate circular shape of the CO2 plume in plane view (Fig. 6B), which justifies using a radial mesh geometry.

Hydraulic initial and boundary conditions.--- The hydrologic parameters used in the simulations are presented in Table 5. Sand and shale formations are homogeneous. Relative permeability models are fitted from core measurements (SACS2, 2002). Injection of carbon dioxide is simulated at 30 kg/sec for 25 years. The initial pressure is 90 bars at the top of the formation, which corresponds to a depth of about 900 m. Hydrostatic pressure is imposed in the outermost column of the mesh.

Geochemical initial conditions.--- Sand and shale mineralogies and formation waters for the 2D model are identical to the batch system considered previously. A low salinity value of 32 g/l is assumed for the formation water both in the sand and the shale.

Short-term simulation results (injection period, 25 years)

Gas saturations and mass fractions of dissolved CO_2 (mass of CO_2 dissolved divided by mass of aqueous phase)) are plotted in Fig. 7 after 3 years and at the end of the injection period (25 years). The gas bubble representing the supercritical CO_2 extends laterally about 300 m away from the injection point, consistent with the seismic observations. The presence of the four intra-shale aquifers gives rise to CO_2 accumulations at four different depths and slows the upward migration of CO_2. The dissolution of gas in the brine produces a maximum dissolved CO_2 mass fraction of 0.052. CO_2 dissolution slightly increases brine density and gives rise to a negative (downward) buoyancy force. At the end of the 25 year injection period, a slight downward migration of the brine enriched in CO_2 can be noted, especially near the top and between 120 m depth and the bottom of the formation.

Dissolution of CO_2 makes the brine more acidic. pH drops to a value of 5.13 inside the gas bubble, which results from buffering due to calcite dissolution (Fig. 8). In the short term acidification occurs mainly in the area where supercritical CO_2 is present. Brine convection and mixing become important in later stages, causing pH changes in regions not invaded by gaseous CO_2 (see below).

The dissolution of calcite is less pronounced in the shales (~5 moles per m^3 of rock) than in the sands (up to 20 moles). Calcite precipitates below each shale layer at the interface between the CO_2 saturated brine and the initial brine, due to mixing of different waters in these regions.

Minor alumino-silicate alteration such as chlorite, albite and muscovite dissolution is also observed during the injection period (results not shown). Also, a small amount of reactions occurs in regions not affected by CO_2 injection. This corresponds to a slight deviation of initial

speciation from equilibrium, as was explained previously. Changes in porosity remain minor (less than 1%), indicating a weak overall chemical reactivity in the media.

Long-term simulation results (10 000 years)

Long-term simulations of gas bubble evolution and dissolved carbon dioxide are shown in Fig. 9. After injection, the upward migration of the supercritical CO_2 occurs quickly, and most of the supercritical CO_2 accumulates just below the cap rock, except for the residual CO_2 that is trapped in sediments. The CO_2 plume extends to a maximum radius of 2,000 m around the injection point. CO_2 starts to dissolve in the brine, and the free gas is completely dissolved after 6,000 years. The brine with dissolved CO_2 tends to migrate downward as it has approximately 10 kg/m^3 larger denser than brine without CO_2. Molecular diffusion from the gas bubble to the brine creates a hydro-dynamically unstable layer leading to the development of convective currents in the formation. The brine containing dissolved CO_2 is carried downward and is replaced by brine with less CO_2. Streamlines of fluid migration showing convective cells are represented in Fig. 10 after 2,000 years of simulation. The slow brine convection accelerates dissolution of the gas bubble. This process has been simulated previously and was compared with laboratory measurements (Lindeberg and Bergmo, 2002). It is interesting that major brine down-flow develops along the corridor where the supercritical CO_2 had ascended at earlier time (Fig. 9). After 10,000 years, a large volume near the bottom of the formation contains brine with dissolved CO_2 out to a radius of 4,000 m.

The role of convective mixing is crucial for the long term CO_2 dissolution. Investigations of this convective instability have been conducted to determine the Rayleigh-Darcy number characterizing timescales and wavelength of the convection (Ennis-King and Paterson, 2003, Lindeberg and Bergmo, 2002). In the case of a very thick slab of CO_2 overlying the formation brine, the solution of the scaled equations was shown to depend only on the permeability anisotropy ratio (Ennis-King and Paterson, 2003). Critical parameters like onset and wavelength

of instability can be calculated analytically for simple cases. In the context of geologic storage of carbon dioxide, the most important time scale is the mixing time t_{mix} required for the entire layer of gas to dissolve:

$$t_{mix} \approx \frac{\alpha L \mu}{k_v \Delta \rho g} \tag{5}$$

Here α is the density ratio of gas to brine, L is the thickness of the initial gas layer, μ is the viscosity, k_v the vertical permeability, $\Delta\rho$ is the density difference between brine with and without dissolved CO_2, and g is the acceleration of gravity. Ennis-King and Paterson (2003) consider this result as an underestimate due to the dilution of the fingers as they propagate. Mixing by pure diffusion would be a much slower process with a time scale of $(\alpha L)^2/D$ where D is the diffusion coefficient.

Using typical parameters ($\phi=0.2$, $\mu=5x10^{-4}$ Pa s, $k_V=10^{-15}$-10^{-14} m², $\Delta\rho=10$ kg m^{-3}, $L=10$ m and $\alpha=10$) for a likely storage site, values of t_{mix} range from 1,600 to 16,000 years. Estimates by Lindeberg and Bergmo (2002) for the CO_2 gas bubble at Sleipner from a 3D model provided a mixing time of about 7,000 years for an average $k_v=200$ mD.

The process of gas dissolution and subsequent buoyant convection and mixing of brine involves a range of spatial scales. Accurate spatial resolution requires extremely fine gridding in 3D (Ennis-King and others, 2002), which currently is impractical for field-scale simulations. Our 2D R-Z model is relatively coarse and furthermore imposes a cylindrical symmetry on the convection process. Simulations of CO_2 injection at Sleipner using a homogeneous 3D model have shown that the fingering and convection behavior during the mixing process has approximate cylindrical symmetry (Frangeul and others, 2004). Furthermore, our model achieves a mixing time of approximately 7,000 years that is consistent with the 3D model of Lindeberg and Bergmo (2002). These comparisons suggest that our model should be able to capture in an approximate way the effects of brine convection and mixing on water chemistry.

The geochemical evolution is shown in figures 11 to 20 by plotting pH and changes in mineral abundance over time. Due to transport effects, the long-term chemical interactions are significantly different from the behavior seen in the batch system. Dissolution of minerals in the shales can mobilize elements that are subsequently transported through convective flow to the sands, where they can participate in geochemical interactions different from those identified in the batch model. The interaction between flow and geochemical reactions and its impact on the overall reactivity can be accurately assessed only through coupled modeling, although this significantly complicates the interpretation of results.

For the interpretation of the long-term reactivity, the evolution of the acidity is crucial, which is directly linked to the amount of CO_2 dissolved in the brine. Fig. 11 shows that dissolution of CO_2 increases the acidity of the brine, which is buffered by carbonate dissolution so that the pH stabilizes at a value of 5.13. This pH value prevails in the region of ascending flow of supercritical CO_2 (500 years), is subsequently established in a region just below the cap rock (between 500 and 1,000 years), and subsequently extends downward (5,000 years). However in most of the region with downward flowing brine pH is somewhat higher because much of the dissolved CO_2 is consumed by geochemical reactions. After 10,000 years low pH values are encountered mainly at the base of the reservoir close to the injection point. One can notice also that in the shale layers initial pH values are raising faster than in the sand layers, which is reinforced by the fact that the initial pH in the shales is higher than in the sands. Due to the fact that the porosity in the shales is much lower, the amount of dissolved CO_2 in the pores is also lower, allowing it to be consumed much faster than in the sands, and causing pH to increase. This latter effect is crucial for interpreting the geochemical interactions, as will be seen below.

Four main types of interactions can be identified.

(i) Calcite dissolution and precipitation – Calcite dissolution occurs mainly in the region above the injection point and at the top of the reservoir just below the cap rock, that is where CO_2 rich brine is present that triggers acid attack on the carbonates. Calcite precipitation occurs

also at low pH in all the shales cross-cut by the main up-flow zone above the injection point, as well as in the top shale layer where brine with low pH is convecting downward. The precipitation of calcite in the shales is a consequence of sand-shale cross-flow and a slight pH difference between the shales and the sands (as indicated in the batch results). Downward flow of brine mobilizes Ca through calcite dissolution in the sands, which leads to super-saturation with respect to calcite when this brine subsequently passes through a shale layer with a slightly higher pH. As a consequence the Ca concentration in the brine declines, providing for additional calcite dissolution when the brine enters the next sand layer below. The effect is most pronounced in the top shale (fig. 12), because the acidity of the brine diminishes overall as it migrates downward, reducing its ability to dissolve calcite in the sands.

Additional calcite precipitation occurs at a later stage near the base of the reservoir where pH slowly increases due to CO_2 consumption in other reactions (see below), thereby increasing the saturation index of calcite.

(ii) Albite alteration – Albite dissolution according to reaction (b) occurs in both batch models, with some alteration in the sands (up to 10 moles per m^3 of rock medium), and stronger alteration in the shales (up to 80 moles per m^3 of rock medium). This is consistent with the observation in the 2D-model (fig. 13), where albite alteration is occurring in the entire region that becomes acidified. Alteration is most intense in the downward limbs of brine convection and in the shale layers. However the formation of chalcedony (Fig. 14) and dawsonite (Fig. 16), which are the reaction products of albite alteration, occurs mainly in the sands (up to 35 and 80 moles per m^3 of rock medium respectively). No dawsonite precipitation occurs in the shales, and the precipitation of chalcedony there is linked to other reactions (see below). Due to the convective flow regime, dissolution and precipitation processes are separated in space. Both SiO_2 and Na are mobilized through albite dissolution in the shales and are re-precipitated as dawsonite and chalcedony in the sands in regions where pH is low.

(iii) Chlorite alteration - Chlorite dissolution (Fig. 15) occurs mainly in the shales in the low pH areas, where the main downward convection cross-cuts the shales. This is consistent with the observations in the batch models. Chlorite dissolution leads to the precipitation of siderite and kaolinite (reaction a), and a strong correlation exists with the precipitation patterns for these minerals (Fig. 20 and Fig. 17 respectively). In this case dissolution and precipitation are not spatially separated as had been the case for the albite alteration. However, the increased Mg from the dissolution of chlorite is mobilized away from the clay layers. As a consequence, no dolomite precipitation takes place, which is different from the batch model. The chlorite dissolution pattern is strongly correlated with the calcite precipitation pattern. Indeed in shales where high Ca concentrations are present, chlorite dissolution is stimulated (see reaction a). Also in the sands the saturation point for dolomite is not reached, and elevated Mg concentrations are maintained.

The dissolution of chlorite is strongly dependent on the pH, as was already pointed out for the batch model of the shales. When pH rises, the reaction can proceed in the reverse direction, leading to the precipitation of chlorite and the dissolution of siderite and kaolinite. This can be observed in some regions of the descending brine, with more intense re-precipitation in the intercalating clay layers (up to 10 moles per m^3 of rock medium). The re-precipitation is aided by elevated Mg concentration in the brine and does not occur in shales where high Ca concentrations are present due to calcite dissolution in the overlying sand layer.

(iiii) Muscovite alteration- the alteration of muscovite (reaction (c) in Fig. 19) is only indirectly linked to CO_2 interactions, in that it does not consume CO_2, but is favored by increased SiO_2 concentrations in the brine that arise from albite or chlorite alteration. Muscovite dissolution occurs mainly in the shale layers and is strongly correlated with the albite dissolution pattern. Muscovite alteration leads to the precipitation of kaolinite (Fig. 17), which is confirmed by a strong correlation with the kaolinite precipitation pattern. Furthermore, muscovite alteration induces the precipitation of k-feldspar as was noted in the batch model for the shales. Although

k-feldspar precipitates in the shales (Fig. 18), a large fraction of the K is mobilized and transported downward, leading to some k-feldspar precipitation in the adjacent sand layers.

Some background chemical reactivity is noticeable as well, due to the initial disequilibrium between the brine composition and the formation water (see above). This activity includes minor calcite and chlorite precipitation, and albite dissolution in the shales.

Amount of CO_2 stored and induced porosity changes.--- Fig. 21 shows a mass balance of carbon dioxide in mineral, supercritical and aqueous phases. From this plot it is clear that mineral trapping plays only a minor role, although it increases slowly with time and therefore contributes to long-term stability of the storage process. At the end of the simulation (10,000 years), no gaseous CO_2 remains in the aquifer. Approximately 5 % of the injected mass has been taken up by minerals, while the remaining 95 % has been dissolved in the brine. Dissolution is more rapid during the injection phase, where after 25 years 11 % of the injected mass has been dissolved while after 1,000 years this value reaches only 30 %. In Fig. 22 the spatial distribution of CO_2 stored in minerals is shown after 10,000 years. A maximum value of 20 kg of CO_2 per m^3 of medium is reached in one location in the upper clay layer. The simulated mineral sequestration occurs mainly at the top of the reservoir and in the major downward convection zone above the injection point.

The induced porosity changes are minor (Fig. 23), with a porosity decrease less than 2.5 % in the sands, while in the shales an increase of up to 15 % is obtained. This illustrates the importance of coupled transport and chemical reaction modeling: in the shales the porosity change is opposite to what was seen in the batch modeling.

Sensitivity analysis

Reactive transport modeling requires the use of many parameters, many of which are not well known because of the complexity of the geological system studied. Lindeberg and Bergmo (2002) studied the impact of the vertical permeability on the dissolution of CO_2 in the brine at Sleipner. They showed that lower vertical permeability implies slower downward migration of

the dissolved CO_2, so that dissolution of the gas bubble is slowed also. Sensitivity analyses on the geochemical properties of the mineral assemblage were performed by Xu and others (2005). Dawsonite precipitation kinetics was identified as the most significant issue in the mineral sequestration of CO_2 in the sandstone-shale system studied. The main uncertainty relates to the reactive surface area, and many assumptions have to be made because of a lack of reliable data. Kumar and others (2004) studied a synthetic reservoir model and evaluated impacts of hydrodynamic parameters on the amount of CO_2 stored. Sensitivity studies were performed for average permeability, the ratio of vertical to horizontal permeability, salinity, temperature, aquifer dip angle, and residual gas saturation. Residual gas saturation was shown to play an important role. For small values of residual gas saturation, a greater amount of gas remains mobile, which leads to increased contact between CO_2 and brine. This in turn leads to increased dissolution of CO_2 in brine. They confirmed this analysis by simulating CO_2 injection over a period of 10 years.

Ennis-King and others (2002) extended this analysis by showing that the residual water saturation S_{wr} is the most sensitive parameter during the injection phase. As the gas displaces formation water, the residual water will be saturated with CO_2 and so a greater S_{wr} value allows for more gas dissolution. Comparison between 2D and 3D meshes and with radial or planar geometry showed sensitivity of the CO_2 dissolution on mesh refinement.

We have performed two simulations to study the sensitivity of CO_2 storage on (i) the residual gas saturation and (ii) the mesh heterogeneity. More work is needed in the future to provide a more comprehensive sensitivity analysis. In the following, the base case corresponding to the simulation previously presented will be called “Case 1,” the simulation performed with a revised residual gas saturation “Case 2,” and the simulation performed with a refined mesh “Case 3”.

Case 2: Smaller residual gas saturation.--- In the previous model a value of 0.20 was assigned which is considered high and corresponds to an efficient residual gas trapping process.

In the new simulation a smaller value of 0.05 is selected while the mesh is kept unchanged from Case 1.

Case 3: Refined Mesh.--- The new mesh was modified only in the radial direction, while vertical discretization was kept the same as in Case 1. In the radial direction, the new mesh has 20 cells with 15 m radial increment near the well followed by 30 cells with 60 m increment and a logarithmic radial distance progression for another 10 cells to reach a maximum radius of 100 km from the injection point. This mesh is more refined than the previous one within 2 km radius of the injection zone, where most of the multiphase effects take place, while it is coarser at larger distance.

Results.--- Results for gaseous and dissolved carbon dioxide for Cases 2 and 3 are plotted in figures 24 and 25, respectively, at times of 50, 1,000, 2,000, 5,000 and 10,000 years. A comparison of mass balances between the three cases is shown in Fig. 26. It is seen that differences between the cases are minor.

The lower value of residual gas saturation in Case 2 leads to more rapid migration of the gas bubble to the top of the formation. During the injection phase, dissolution is faster than in Case 1, in agreement with trends noted by Kumar and others (2004) and Ennis-King and others (2002). After 3 years of injection, 21 % of the CO_2 has been dissolved in Case 2 (Fig. 26) compared to 17 % for Case 1. This trend reverses for the long term storage phase, and after 1,000 years 23 % of CO_2 has been dissolved in Case 2 compared to 30 % in Case 1. After 50 years the volume occupied by the gas phase is smaller in Case 2 than in Case 1 (figures 24 and 9), so that less CO_2 is in contact with brines and dissolution becomes slower. At the end of the simulation, the downward convection is stronger in Case 2 than in Case 1.

Three years after injection, Case 3 predicts a CO_2 dissolution of 15 % which is slightly lower than in Case 1 (Fig. 25). Dissolution remains similar up to 1000 years, and subsequently becomes slightly stronger. This behavior is consistent with the idea that mesh refinement should enhance local density contrasts and strengthen the convection process.

SUMMARY AND CONCLUSION

A 2D radially symmetric reactive chemical transport model for the Sleipner CO_2 injection project has been developed. A 25 year injection period was simulated followed by a 10,000 year storage period that allowed to describe the evolution of the three main trapping processes of carbon dioxide: structural, dissolution and mineral trapping. The system was modeled as consisting of alternating highly permeable sands, separated by semi-permeable shales with different mineralogy.

Our simulations indicate that the geochemical reactivity of the Utsira formation is rather low, so that mineral trapping makes only minor contributions to CO_2 storage. Solubility trapping is shown to be the dominant long-term storage mechanism and is essentially complete after 5000 years. Physical and chemical heterogeneity play important roles in the geochemical evolution and associated changes in porosity. Our results suggest that the Utsira sand is unlikely to undergo major chemical changes as a consequence of CO_2 injection. Anticipated porosity changes are relatively minor, with a slight long-term decrease expected in the sands and a more significant increase in the shales.

Density differences between brines with different dissolved CO_2 concentrations give rise to convective flows that cross the shale layers, mobilizing species that subsequently promote precipitation further downstream. Processes in which dissolution of minerals occurs in one region while precipitation occurs in another region with different mineralogy can only be analyzed and modeled by coupling flow and transport with chemical reactions. The strong interplay between multiphase and density-dependent flows with rock-fluid interactions makes it difficult to interpret modeled results in terms of a few dominant reactions. Separate batch geochemical modeling provides useful guidance for interpretation, but our results show that in some cases the coupling to transport can give rise to qualitatively different behavior than seen in batch models.

Reactive transport modeling requires numerous parameters that typically are only partially known. Limited sensitivity studies on residual gas saturation and mesh resolution showed minor impacts on long-term storage predictions. For lower residual gas saturation the mobility of the free gas phase is higher and therefore the spreading and dissolution of the supercritical CO_2 is accelerated. Lower mesh resolution will underestimate CO_2 dissolution rate.

Coupled modeling of geochemical reactions with multiphase flow and transport remains a challenging task. Further improvements are needed to better represent processes such as thermal coupling, solid solution kinetics, and redox phenomena, and also to reduce CPU time and memory requirements for such complex studies.

ACKNOWLEDGMENTS

Pascal Audigane, Irina Gaus and Isabelle Czernichowski-Lauriol thank the CO2STORE consortium for their funding and their permission to publish this work. CO2STORE is funded by the EU, by industry partners Statoil, BP, ExxonMobil, Norsk Hydro, Total, Energi E2, PEL, IMN, Schlumberger technology and Vattenfall, and by national governments. Research and Development partners are BGS, BGR, NGU, BRGM, GEUS, IFP, TNO-NITG and SINTEF. Karsten Pruess and Tianfu Xu acknowledge support from the Zero Emission Research and Technology project (ZERT) through Contract No. DE-AC02-05CH11231 with the U.S. Department of Energy.

REFERENCES

Appelo, C.A.J. and Postma, D., 1993, Geochemistry, groundwater and pollution: Rotterdam, The Netherlands, Balkema, 536 p.

Arts, R., Chadwick, A., Eiken, O., 2004, Recent time-lapse seismic data show no indication of leakage at the Sleipner CO_2 -injection site, *in* Rubin, E.S., Keith, D.W. and Gilboy, C.F., editors, Proceedings of the 7th International Conference on Greenhouse Gas Control Technologies, Volume 1, Peer-Reviewed Papers and Plenary Presentations: Cheltenham, UK, IEA Greenhouse Gas Program.

Baker, J.C., Bai, G.P., Hamilton, P.J., Golding, S.D. and Keene, J.B., 1995, Continental-scale magmatic carbon dioxide seepage recorded by dawsonite in the Bowen-Gunnedah-Sydney Basin System, eastern Australia: Journal of Sedimentary Petrology, v. 65, A, p. 22-53.

Battistelli, A., Calore, C., Pruess, K., 1997, The simulator TOUGH2/EWASG for modeling geothermal reservoirs with brines and non condensable gas: Geothermics, v. 26, (4), p. 437-464.

Bjørlykke, K., Nedkvitne, T., Mogens, R. and Girish C.S., 1992, Diagenetic processes in the Brent Group (Middle Jurassic) reservoir of the North Sea: an overview, *in* Morton, A.C., Haszeldine, R.S., Giles, M.R. and Brown, S., editors, Geology of the Brent Group: Geological Society Special Publication, v. 61, p. 263-287.

Blum, A.E., Stillings, L.L., 1995, Feldspar dissolution kinetics, Chapter 7 of chemical weathering rate of silicate minerals, *in* White, A.F., Brantley, S.L., editors: Washington, DC , Mineral Society of America annual meeting, v. 31, p. 291-351.

Bøe, R. and Zweigel, P., 2001, Characterization of the Nordland shale in the Sleipner area by XRD analysis—a contribution to the Saline Aquifer CO_2 Storage (SACS) project: Trondhiem, Norway, Confidential SINTEF Report 33.0764.00/01/01.

Czernichowski-Lauriol, I., Sanjuan, B., Rochelle, C., Bateman, K., Pearce, J., Blackwell, P., 1996, Inorganic geochemistry, Chapter 7 *in*, The underground disposal of carbon dioxide, S. Holloway, editor: Final Report CT92-0031 of JOULE II Project.

Czernichowski-Lauriol, I., Rochelle, C.A., Brosse, E., Springer, N., Bateman, K., Kervévan, Ch., 2002, Reactivity of injected CO_2 with the Utsira sand reservoir at Sleipner: Proceedings of the 6th International Conference on Greenhouse Gas Control Technology: Kyoto, Japan, 1-4 October 2002.

Ennis-King, J., Gibson-Poole, C.M., Lang, S.C., Paterson, L., 2002, Long-term numerical simulation of geological storage of CO_2 in the Petrel sub-basin, North West Australia, *in* APRC /GEODISC Project Paper http://www.apcrc.com.au/GEODISC%20PDFs/Ennis-King%20Long%20Term%20Simulation%20paper.pdf.

Ennis-King, J. and L. Paterson, 2003, Role of Convective Mixing in the Long-Term Storage of Carbon Dioxide in Deep Saline Formations: Paper SPE-84344, presented at the Society of Petroleum Engineers Annual Fall Technical Conference and Exhibition, Denver, CO, October 2003, Paper SPE-84344.

Forster, C., Pasala, S., Deo, M., Shipton, Z., Evans, J., Parry, W., 2004, Analysis of naturally occurring CO_2 systems, and simulation of the impacts of faults on CO_2 injection into sandstone aquifers, *in* Rubin, E.S., Keith, D.W. and Gilboy, C.F., editors, Proceedings of the 7th International Conference on Greenhouse Gas Control Technologies, Volume 1, Peer-Reviewed Papers and Plenary Presentations: Cheltenham, UK, IEA Greenhouse Gas Program.

Frangeul, J., Nghiem, L., Emmanuel, C., Thibeau, S., 2004, Sleipner/Utsira CO_2 geological storage: full field flow and geochemical coupling to assess the long term fate of the CO_2: Proceedings AAPG Annual Conference, Dallas, Texas, 18-21 April, 2004, Paper AAPG 86278.

Gaus, I., Azaroual, M., Czernichowski-Lauriol, I., 2005, Reactive transport modeling of the impact of CO_2 injection on the clayey cap rock at Sleipner (North Sea): Chemical Geology, v. 217, p. 319-337.

Gaus, I., Le Guern, C., Pearce, J., Pauwels, H., Shepherd, T., Hatziyannis, G., Metaxas, A., 2004, Comparison of long term geochemical interactions at two natural CO_2 -analogues : Montmiral (Southeast basin, France) and Messokampos (Florina basin, Greece) case studies, *in* Rubin, E.S., Keith, D.W. and Gilboy, C.F., editors, Proceedings of the 7th International Conference on Greenhouse Gas Control Technologies, Volume 1, Peer-Reviewed Papers and Plenary Presentations: Cheltenham, UK, IEA Greenhouse Gas Program.

Gunter, W.D., Wiwchar, B., Perkins, E. H., 1997, Aquifer disposal of CO_2 -rich greenhouse gases: extension of the time scale of experiment for CO_2-sequestering reactions by geochemical modeling: Mineralogy and Petrology, v. 59, p. 121-140.

Helgeson , H.C., Kirkham, D.H., 1974, Theoretical prediction of the thermodynamic behavior of aqueous electrolytes at high pressures and temperatures: II. Debye-Hückel parameters for activity coefficients and relative partial molal properties: American Journal of Science, v. 274, p. 1199-1261.

Hitchon, B., 1996, Aquifer Disposal of Carbon Dioxide, Hitchon, B, editor: Sherwood Park, Alberta, Canada, Geoscience Publishing Limited.

Holloway, S., 1997, An overview of the underground disposal of carbon dioxide: Energy Conversion and Management., v. 38, p. 193-198.

Holloway, S., 2002, Underground sequestration of carbon dioxide - a viable greenhouse gas mitigation option: Proceedings of the 5th International Symposium on CO_2 Fixation and Efficient Utilization of Energy and the 4th International World Energy System Conference: Tokyo Institute of Technology, Tokyo, Japan, March 4-6, 2002, p. 373-380.

IPCC, 2002, Proceedings of the IPCC Workshop on carbon dioxide capture and storage: Regina, Canada, 18-12 November 2002.

IEAGHG, 2005, IEA Green House Gas R&D program: Green House Issues, number 76, January 2005, http://www.ieagreen.org.uk/jan76.htm.

Johnson, J.W., Oelkers, E.H., Helgeson, H.C., 1992, SUPCRT92: A software package for calculating the standard molal thermodynamic properties of minerals, gases, aqueous species, and reactions from 1 to 5000 bars and 0 to 1000°C: Computers and Geosciences, v.18, 7, p 899-947.

Johnson, J.W., Lundeen, S.R., 1994, GEMBOCHS thermodynamic data files for use with the EQ3/6 software package: Lawrence Livermore National Laboratory, Livermore, California, LLNL-YMP Milestone report MOL72, 99 p.

Johnson, J.W., Nitao, J.J., Steefel, C., Knaus, K.G., 2001, Reactive transport modeling of geological CO_2 sequestration in saline aquifers; The influence of intra-aquifer shales and the relative effectiveness of structural, solubility, and mineral trapping during prograde and retrograde sequestration: First annual conference on carbon sequestration, may 14-17th, , Washington, 2001.

Kemp, S.J., Pearce, J.M., Steadman, .J., 2002, Mineralogical, geochemical, and petrographical characterization of Nordland Shale cores from well 15/9-A-11, Sleipner field, northern North Sea: British Geological Survey Commissioned Report, CR/02/313., 40 p.

Kumar, A., Noh, M., Pope, G.A., Sepehrnoori, K., Bryant, S., Lake, L.W. 2004, Reservoir simulation of CO_2 storage in deep saline aquifers: Paper SPE 89343 presented at the SPE/DOE 14th Symposium on Improved Oil Recovery, Tulsa, Oklahoma, USA, 17-21 April 2004, Paper SPE-89343.

Lagneau, V., Pipart, A., Catalette, H., 2005, Reactive transport modeling of CO_2 sequestration in deep saline aquifers: Oil and Gas Science Technology- Rev. IFP, v. 60, 2, p. 231-247.

Lasaga, A.C., 1984, Chemical kinetics of water-rock interactions: Journal of Geophysical Research, v. 89, p. 4009-4025.

Lindeberg, E., Causse, E., Ghaderi, A., 1999, Evaluation of to what extent CO_2 accumulations in the Utsira formations are possible to quantify by seismic by August 1999: Trondhiem, Norway, Restricted SINTEF Petroleum Research Report 54.5148.00/01/99, 13 p.

Lindeberg, E., Zweigel, P., Bergmo, P., Ghaderi, A., Lothe, A., 2000, Prediction of CO_2 dispersal pattern improved by geology and reservoir simulation and verified by time lapse seismic: Proceedings of the 5th International Conference on Greenhouse Gas Control Technologies, Cairns (Australia), August 2000.

Lindeberg, E., Bergmo, P., 2002, The long term fate of CO_2 injected into an aquifer: Proceedings of the 6th International Conference on Greenhouse Gas Control Technology: Kyoto, Japan, 1-4 October 2002.

Malmstrom, M., Banwart, S., Lewenhagen, J., Duro, L., Bruno, J., 1996, The dissolution of biotite and chlorite at 25 °C in the near neutral pH region: Contaminant Hydrology, v. 21, p. 201-213.

Moore, J., Adams, M., Allis, R., Lutz, S. and Rauzi, S., 2003, CO_2 mobility in natural reservoirs beneath the Colorado Plateau and Southern Rocky Mountains: an example from the Springerville-St Johns Field, Arizona and New Mexico: Proceedings of the Second Annual Conference on Carbon Sequestration, 5-8 May, Alexandria VA.

Nagy, K.L., 1995, Dissolution and precipitation kinetics of sheet silicate, in, White, A.F., Brantley, S.L., editors, Chemical Weathering Rates of Silicates Minerals: Mineralogical Society of America, v. 31, p. 173-273.

Narasimhan, T.N., and Witherspoon, P.A., 1976, An integrated finite difference method for analyzing fluid flow in porous media: Water Resources Research, v. 12, p. 57-64.

Nghiem, L., Sammon, P., Grabenstetter, J., Ohkuma, H., 2004, Modeling CO_2 storage in aquifers with a fully-coupled geochemical EOS compositional simulator: Proceedings SPE 89474

for the SPE/DOE 14th Symposium on Improved Oil recovery, Tulsa, Oklahoma, 17-21 April, 2004, Paper SPE-89474.

Nitao, J.J., 1998, Reference manual for the NUFT flow and transport code, version 2.0: Lawrence Livermore National Laboratory, Livermore, California, UCRL-MA-130651, 55 p.

Oldenburg, C., Benson, S., 2002, CO_2 injection for enhanced gas production and carbon sequestration: Proceedings SPE 74367 presented at the SPE International Petroleum Conference and Exhibition, Mexico, 10-12 February 2002, Paper SPE 74367.

Parkhurst, D.L. and Appelo, C.A.J. 1999, User's guide to PHREEQC (version 2)--A computer program for speciation, batch-reaction, one-dimensional transport, and inverse geochemical calculations: U.S. Geological Survey Water-Resources Investigations, Report 99-4259, 312 p.

Pearce, J.M., Holloway, S., Wacker, H., Nelis, M.K., Rochelle, C., Bateman, K., 1996, Natural occurrences as analogues for the geological disposal of carbon dioxide, Energy Conversion and Management, v. 37, p. 1123-1128.

Pearce, J.M., Kemp, S.J., Wetton, P.D., 1999, Mineralogical and petrographical characterization of 1m core from the Utsira formation, Central North Sea: British Geological Survey, Report WG/99/24C.

Pruess, K., 1987, Tough user's guide: Nuclear Regulatory Commission , report NUREG/CR-4645 (also Lawrence Berkeley Laboratory Report LBL-20700, Berkeley, California).

Pruess, K., 1991, TOUGH2 – a general-purpose numerical simulator for multiphase fluid and heat flow: Lawrence Berkeley Laboratory Report LBL-29400, Berkeley, California.

Pruess, K., Xu, T., Apps, J., García, J., 2001, Numerical Modeling of Aquifer Disposal of CO_2: Proceedings SPE66537 presented at the SPE/EPA/DOE Exploration and Production Environmental Conference, San Antonio, Texas, 26-28 February, 2001, Paper SPE66537.

Pruess; K., García, J., 2002, Multiphase flow dynamics during CO_2 disposal into saline aquifers: Environmental Geology, v. 42, p. 282-295.

Pruess, K., 2004, The TOUGH codes- A family of simulation tools for multiphase flow and transport processes in permeable media: Vadose Zone Journal, Special section, Research advances in vadoze zone hydrology through simulations with the TOUGH codes, v. 3, p. 738-746.

Pruess, K., García, J., Kovscek, T., Oldenburg, C., Rutqvist, J. Steefel, C., Xu, T., 2004, Code intercomparison builds confidence in numerical simulation models for geologic disposal of CO_2: Energy, v. 29, p. 1431-1444.

Rochelle, C.A., and Moore, Y.A., 2002, The solubility of supercritical CO_2 into pure water and synthetic Utsira porewater: British Geological Survey Report CR/02/052.

Rochelle, C.A., Bateman, K., Pierce, J.M., 2002, Geochemical interactions between supercritical CO_2 and the Utsira Formation: an experimental study: British Geological Survey Report CR/02/060.

SACS2, 2002, Final Technical Report: EU-contract ENK6-CT-1999-00014.

Stankevich, E.F., Stankevich, Y.F., Batalin,Y.V., 1976, Distribution and origin of dawsonite: Lithology and Mineral Resources, v. 11, (3), p. 359-368.

Steefel, C.I., 2001, GIMRT, version 1.2: Software for modeling multicomponent, multidimensional reactive transport. User's Guide: Livermore, California, Lawrence Livermore National Laboratory Report UCRL-MA-143182, 76 p.

Steefel, C.I., Lasaga, A.C., 1994, A coupled model for transport of multiple chemical species and kinetic precipitation/dissolution reactions with applications to reactive flow in single phase hydrothermal system: American Journal of Science, v. 294, p. 529-592.

Shock, E.L., 1998, An updated and augmented version (slop98.dat) of the original SUPCRT92 database (sprons92.dat). http:/zonvark.wustl.edu/geopig.

Sonnenthal, E.L., Spycher, N., 2001, Drift-Scale coupled processes (DST and THC seep-age) models: AMR N0120/U0110 Rev.01, Yucca Mountain Project, Berkeley, California, Lawrence Berkeley National Laboratory Report.

Tester, J.W., Worley, G.W., Robinson, B.A., Grigsby, C.O., Feerer, J.L., 1994, Correlating quartz dissolution kinetics in pure water from 25° to 625 °C, Geochimica et Cosmochimica Acta,v. 58, p. 2407-2420.

Torp, T.A., Gale, J., 2002, Demonstrating storage of CO_2 in geological reservoirs: the Sleipner and SACS projects: Proceedings of the 6th International Conference on Greenhouse Gas Control Technology: Kyoto, Japan, 1-4 October 2002.

van Genuchten, M. Th., 1980, A closed-form equation for predicting the hydraulic conductivity of unsaturated soils, Soil Science Society of American Journal, v. 44, p. 892-898.

Weir, G., White, S.P., Kissling, W., 1996, Reservoir storage and containment of greenhouse gases: Transport in porous media, v. 23, p. 37-60.

White, S.P., 1995, Multiphase non isothermal transport of systems of reacting chemicals, Water Resource Research, v. 31, p. 1761-1772.

White, S.P., Weir, G., Kissling, W., 2001, Numerical simulation of CO_2 sequestration in natural CO_2 reservoirs on the Colorado Plateau: Proceedings of the 1st National Conference on Carbon Sequestration, Washington D.C., May 2001.

White, S.P., Allis, R.G., Moore, J., Chidsey, T., Morgan, C., Gwynn, W., Adams, M., 2005, Simulation of reactive transport of injected CO_2 on the Colorado Plateau, Utah, USA: Chemical Geology, v. 217, p. 387-405.

Xu, T., Pruess, K., 2001, Modeling multiphase non-isothermal fluid flow and reactive geochemical transport in variably saturated fractured rocks: 1. Methodology: American Journal of Science, v. 301, p. 16-33.

Xu, T., Apps, J., Pruess, K., 2003, Reactive geochemical transport simulation to study mineral trapping for CO_2 disposal in deep arenaceous formations: Journal of Geophysical Research, v. 108, (B2), p. 2071, doi:10.1029/2002JB001979.

Xu, T., Apps, J., Pruess, K., 2004, Numerical simulation of CO_2 disposal by mineral trapping in deep aquifers: Applied geochemistry, v. 19, p. 917-936.

Xu, T., Apps, J., Pruess, K., 2005, Mineral sequestration of a sandstone-shale system: Chemical geology, v. 217, (3-4), p. 295-318.

Xu, T., E.L. Sonnenthal, N. Spycher, and K. Pruess, 2006, TOUGHREACT: A simulation program for non-isothermal multiphase reactive geochemical transport in variably saturated geologic media, Computers & Geosciences, v. 32/2, p. 145-165.

Yeh, G.T., Tripathi, V.S., 1991, A model for simulating transport of reactive multi-species components : Model development and demonstration: Water Resource Research, v. 27, p. 3075-3094.

Zhou, W., Stenhouse, M., Arhtur, R., Whittaker, S., Law, D., Chalaturnyk, R., Jazrawi, W., 2004, The IEA Weyburn CO_2 monitoring project modeling of the long term migration of CO_2 from Weyburn, *in* Rubin, E.S., Keith, D.W. and Gilboy, C.F., editors, Proceedings of the 7th International Conference on Greenhouse Gas Control Technologies, Volume 1, Peer-Reviewed Papers and Plenary Presentations: Cheltenham, UK, IEA Greenhouse Gas Program.

TABLES

Table 1. Mineralogical composition of the Utsira Sand derived from Pearce and others (1999) and its conceptualization in the geochemical model

Nordland shale composition (after Pearce and others, 1999)	Volume fraction	Minerals introduced in the model	Volume fraction
Plagioclase	0.0301	**Albite~low**	0.030
Calcite	0.0674	**Calcite**	0.067
Quartz	0.7633	**Chalcedony**	0.769
Chlorite	0.0133	**Chlorite**	0.013
Mica/Illite	0.0522	**Muscovite**	0.052
K-feldspar	0.0693	**K-feldspar**	0.069
Pyrite	0.0005	Not used	--
Ilmenite	0.0012	Not used	--
Apatite	0.0002	Not used	--
Zeolite	0.0022	Not used	--
Ti Oxides	0.0003	Not used	--
Siderite	--	Siderite	0.000
Kaolinite	--	Kaolinite	0.000
Dolomite-dis	--	Dolomite-dis	0.000
Magnesite	--	Magnesite	0.000
Dawsonite	--	Dawsonite	0.000

Table 2. Mineralogical composition of the Nordland Shale derived from Bøe and Zweigel (2001) and the amounts introduced in the model

Nordland shale composition (after Bøe and Zweigel, 2001)	Volume percent	Minerals introduced in the model	Volume percent
Plagioclase	0.132	**Albite~low**	0.132
Calcite	0.010	**Calcite**	0.010
Quartz	0.228	**Chalcedony**	0.334
Chlorite	0.044	**Chlorite**	0.044
Mica/Illite	0.251	**Muscovite**	0.251
Kaolinite	0.195	**Kaolinite**	0.195
K-feldspar	0.023	**K-feldspar**	0.023
Siderite	0.011	**Siderite**	0.011
Smectite	0.09	Not used	--
Pyrite	0.016	Not used	--
Dolomite-dis	--	Dolomite-dis	0.000
Magnesite	--	Magnesite	0.000
Dawsonite	--	Dawsonite	0.000

Table 3. Initial composition of the formation water in the cap rock

Parameter	Value	Elements	Concentration (M)
Temperature (°C)	37	Al	$0.4542\ 10^{-15}$
pH	7.67	C	$0.1973\ 10^{-01}$
		Ca	$0.3701\ 10^{-03}$
		Cl	$0.5375\ 10^{+00}$
		Fe	$0.4096\ 10^{-14}$
		K	$0.1553\ 10^{-02}$
		Mg	$0.2576\ 10^{-05}$
		Na	$0.5439\ 10^{+00}$
		S	$0.1024\ 10^{-14}$
		Si	$0.1811\ 10^{-03}$

Table 4. List of kinetic rate parameters for minerals considered in the simulations

Mineral	k_{25} (mol $m^{-2}s^{-1}$)	Ea (KJ/mol)	Reference	Surface area (cm^2/g)
Calcite	Equilibrium	--	--	--
Magnesite	Equilibrium	--	--	--
Dawsonite	Equilibrium	--	--	--
Siderite	$1.26\ 10^{-9}$	62.76	Steefel (2001)	9.8
Albite	$1.00\ 10^{-12}$	67.83	Blum and Stillings (1995)	9.8

Chalcedony	$1.26\ 10^{-14}$	87.50	Tester and others (1994)	9.8
Chlorite	$2.51\ 10^{-12}$	62.76	Malmstrom and others (1996)	9.8
Kaolinite	$1.00\ 10^{-13}$	62.76	Nagy (1995)	151.6
Illite	$1.00\ 10^{-13}$	62.76	Set to kaolinite	151.6
K-feldspar	$1.00\ 10^{-12}$	57.78	Blum and Stillings (1995)	9.8
Dolomite-dis	$1.26\ 10^{-9}$	62.76	Set to siderite	9.8

Table 5. Hydrogeological parameters for the 2D model of CO_2 injection at Sleipner with TOUGHREACT

	Sand	Shale
Permeability	3.0 10^{-12} m²	10^{-14} m²
Porosity	0.42	0.1025
Temperature	37°C	37°C
Pore compressibility	4.5 10^{-10} Pa^{-1}	4.5 10^{-10} Pa^{-1}
Relative permeability model:		
. Liquid (Van Genuchten, 1980)		
$k_{rl} = \sqrt{S^*}\left\{1-\left(1-\left[S^*\right]^{1/m}\right)^m\right\}^2$	$S^* = \frac{S_l - S_{lr}}{1-S_{lr}}$	
Residual liquid saturation	$S_{lr} = 0.05$	$S_{lr} = 0.05$
Exponent	$m = 0.75$	$m = 0.75$
. Gas (Corey, 1954)		
$k_{rg} = \begin{cases} 1-k_{rl} & if \quad S_{gr} = 0 \\ \left(1-\hat{S}\right)^2\left(1-\hat{S}^2\right) & if \quad S_{gr} < 0 \end{cases}$	$\hat{S} = \frac{S_l - S_{lr}}{1-S_{lr}-S_{gr}}$	
Residual gas saturation	$S_{gr} = 0.20$	$S_{gr} = 0.20$
Capillary pressure (Van Genuchten, 1980)		
$P_{cap} = -P_0\left(\left[S^*\right]^{-1/m} - 1\right)^{1-m}$	$S^* = \frac{S_l - S_{lr}}{1-S_{lr}}$	
Residual liquid saturation	$S_{lr} = 0.05$	$S_{lr} = 0.05$
Exponent	$m = 0.65$	$m = 0.65$
Coefficient	$P_0 = 1.43kPa$	$P_0 = 1.43kPa$

FIGURES CAPTIONS

Fig. 12. Calcite mineral evolution in moles per m3 of rock medium (negative sign for dissolution, positive sign for precipitation) after 500, 1000, 5000 and 10 000 years, following 25 years of injection of supercritical CO2.

Fig. 13. Albite mineral evolution in moles per m3 of rock medium (negative sign for dissolution, positive sign for precipitation) after 500, 1000, 5000 and 10 000 years, following 25 years of injection of supercritical CO2.

Fig. 14. Chalcedony mineral evolution in moles per m3 of rock medium (negative sign for dissolution, positive sign for precipitation) after 500, 1000, 5000 and 10 000 years, following 25 years of injection of supercritical CO2.

Fig. 15. Chlorite mineral evolution in moles per m3 of rock medium (negative sign for dissolution, positive sign for precipitation) simulated after 500, 1000, 5000 and 10 000 years, following 25 years of injection of supercritical CO2.

Fig. 16. Dawsonite mineral evolution in moles per m3 of rock medium (negative sign for dissolution, positive sign for precipitation) after 500, 1000, 5000 and 10 000 years, following 25 years of injection of supercritical CO2.

Fig. 17. Kaolinite mineral evolution in moles per m3 of rock medium (negative sign for dissolution, positive sign for precipitation) after 500, 1000, 5000 and 10 000 years, following 25 years of injection of supercritical CO2.

Fig. 18. K-feldspar mineral evolution in moles per m3 of rock medium (negative sign for dissolution, positive sign for precipitation) after 500, 1000, 5000 and 10 000 years, following 25 years of injection of supercritical CO2.

Fig. 19. Muscovite mineral evolution in moles per m3 of rock medium (negative sign for dissolution, positive sign for precipitation) after 500, 1000, 5000 and 10 000 years, following 25 years of injection of supercritical CO2.

Fig. 20. Siderite mineral evolution in moles per m3 of rock medium (negative sign for dissolution, positive sign for precipitation) after 500, 1000, 5000 and 10 000 years, following 25 years of injection of supercritical CO2.

Fig. 21. Total amounts of carbon dioxide present as a free (supercritical) gas phase, dissolved in the aqueous phase, and sequestered in minerals.

Fig. 22. Spatial distribution of the amount of carbon dioxide sequestered as minerals (SMco2), in kg of CO2 per m3 of rock.

Fig. 23. Porosity changes after 10 000 years of simulation. dporo = 100 x (ϕ-ϕinit)/ϕinit. A porosity increase (dporo>0) of up to 15 % occurs in the shales, while a slight decrease (dporo<0) of less than 5 % is seen in the sands.

Fig. 24. Results obtained with residual gas saturation reduced to 0.05 (Case 2). Supercritical CO2 gas bubble migration and mass fraction of the dissolved gas in the brine are shown for up to10 000 years, following 25 years of injection of supercritical CO2.

Fig. 25. Results obtained with the new mesh (case 3). Supercritical CO2 gas bubble migration and mass fraction of the dissolved gas in the brine are shown for up to10 000 years, following 25 years of injection of supercritical CO2.

Fig. 26. Comparison of CO2 inventories in the different phases for three different cases: Case 1 with the original mesh and a residual saturation of 0.20, Case 2 with the same mesh and a reduced residual gas saturation of 0.05, and Case 3 with a residual gas saturation of 0.20 and a mesh that is more refined near the injection point.

FIGURES

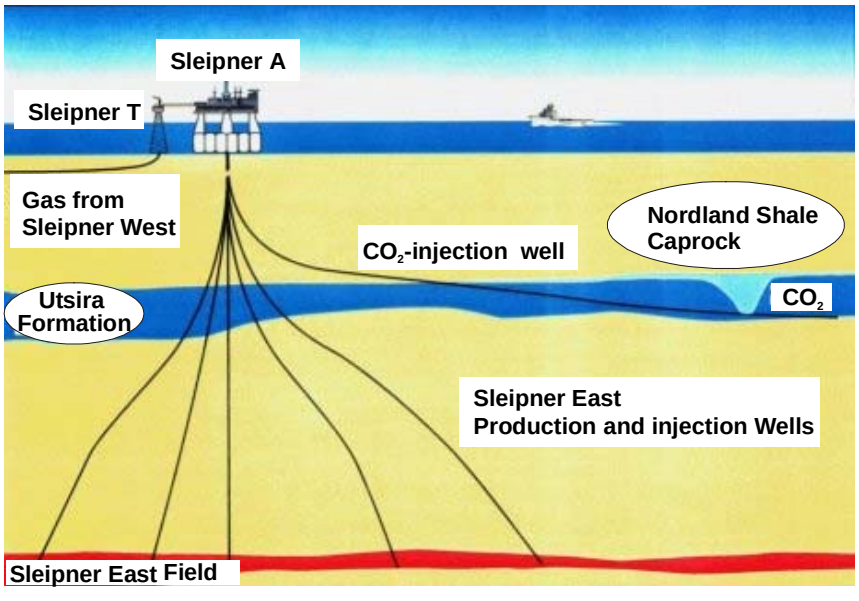

Fig. 1. Cross section of CO_2 injection in the Utsira Formation at Sleipner (SACS, 2002).

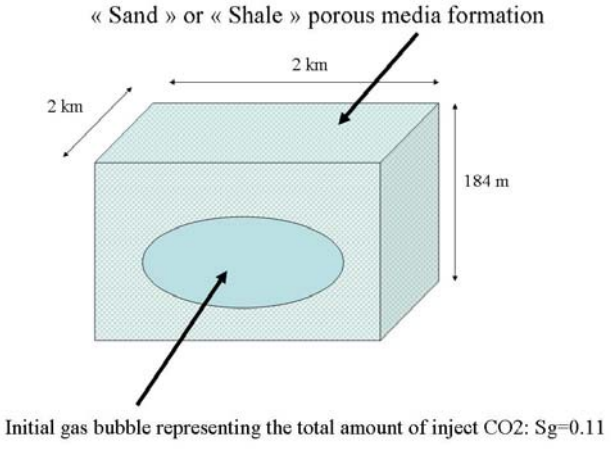

Fig. 2. Schematic of the volume of rock used for batch geochemical simulations.

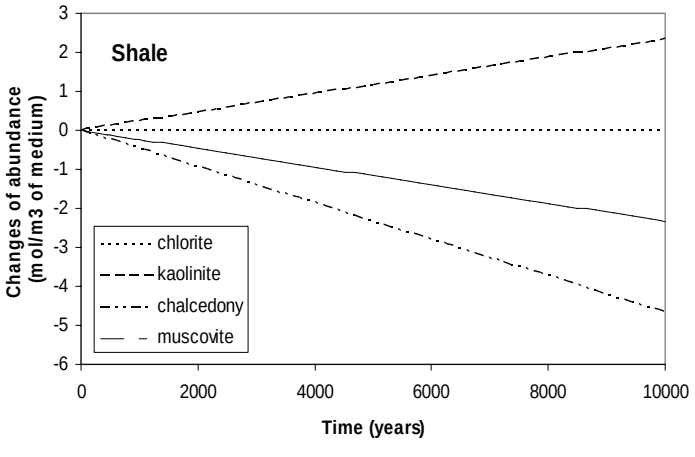

Fig. 3. Kinetic batch modeling in the shale formation prior to CO_2 injection. Evolution of the most relevant minerals.

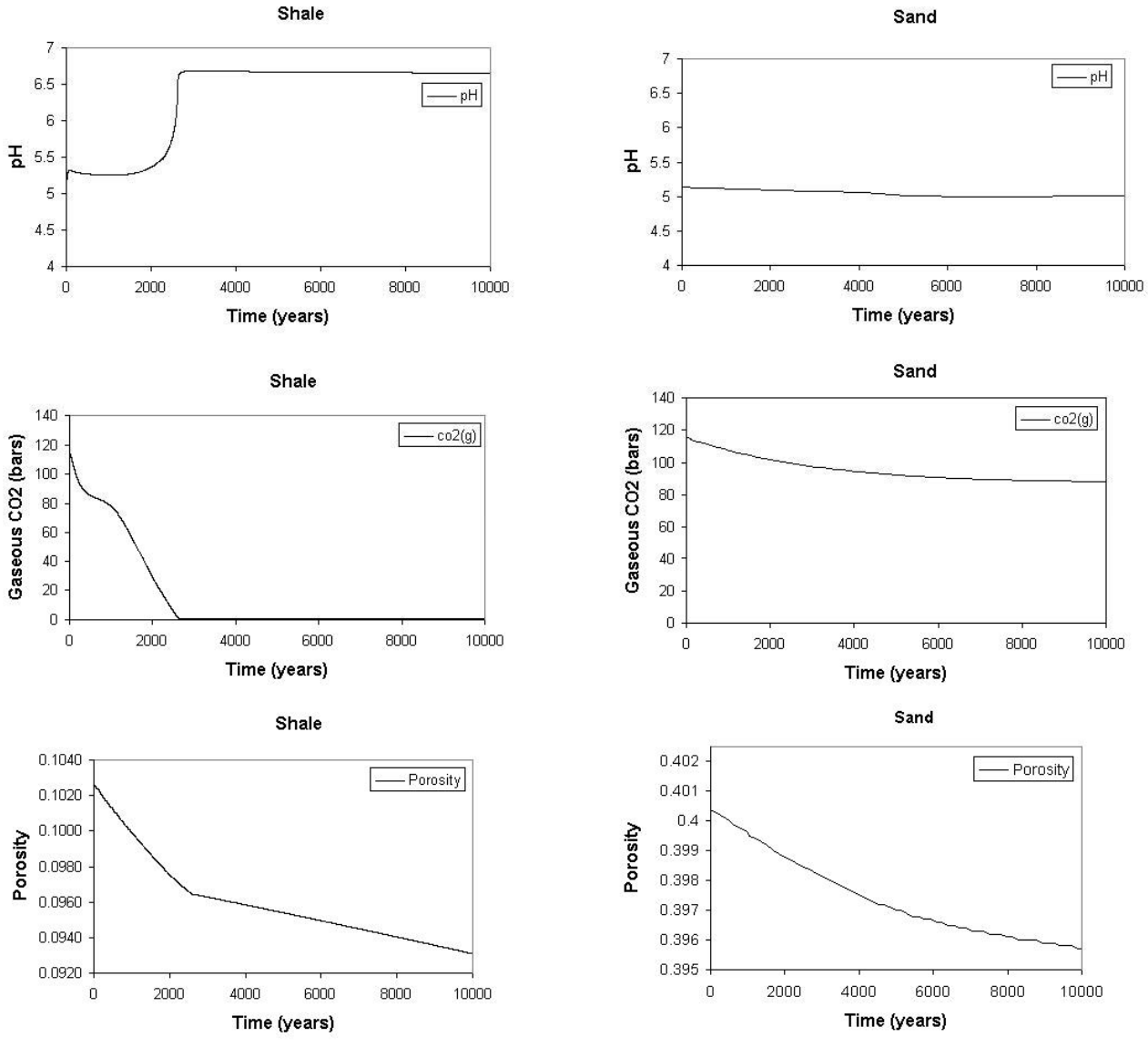

Fig. 4. Evolution of pH, porosity, and gaseous carbon dioxide during batch geochemical modeling over 10,000 years in the shale and sand formations.

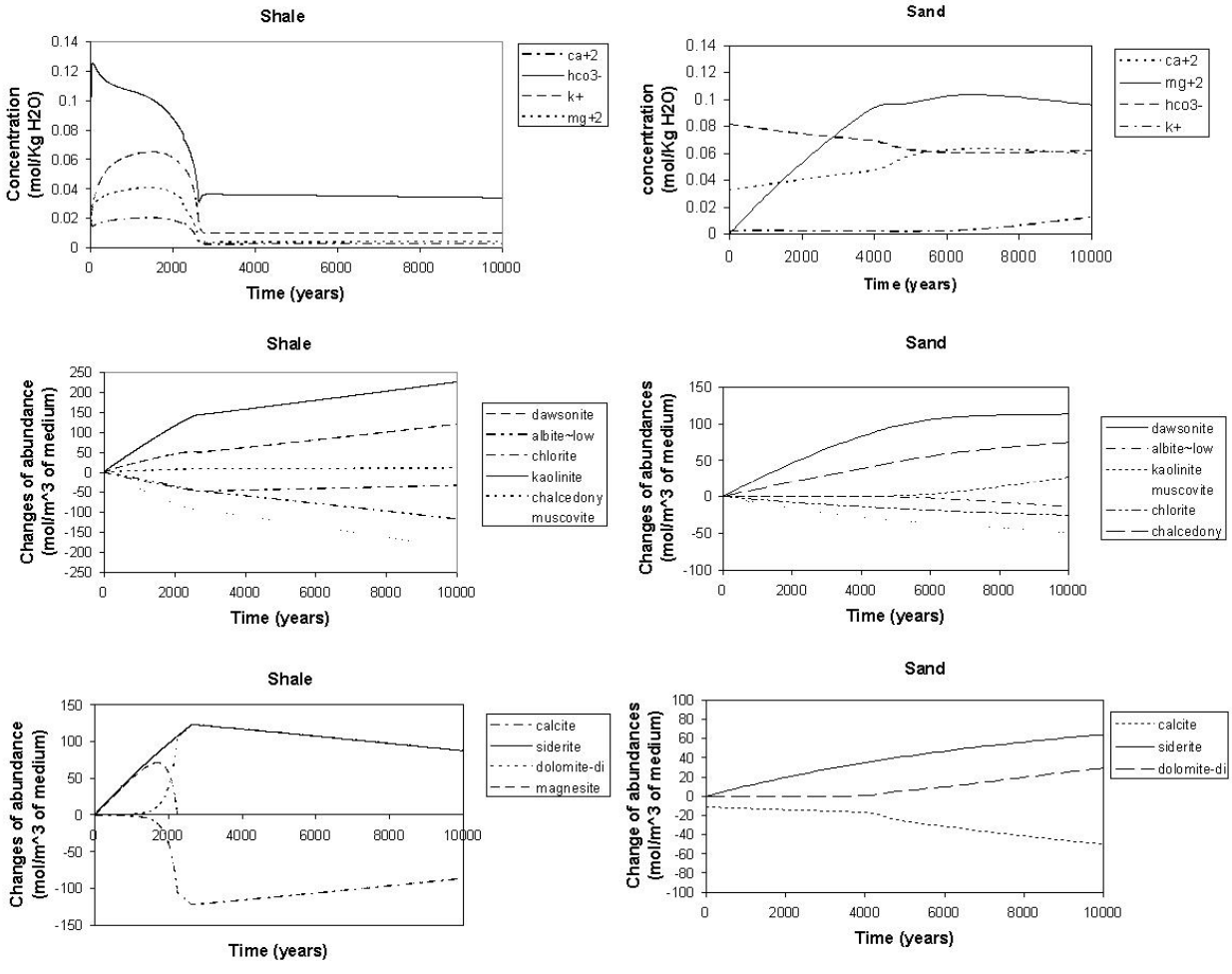

Fig. 5. Evolution of aqueous species and minerals for the batch geochemical model over 10,000 years in the shale and sand formations.

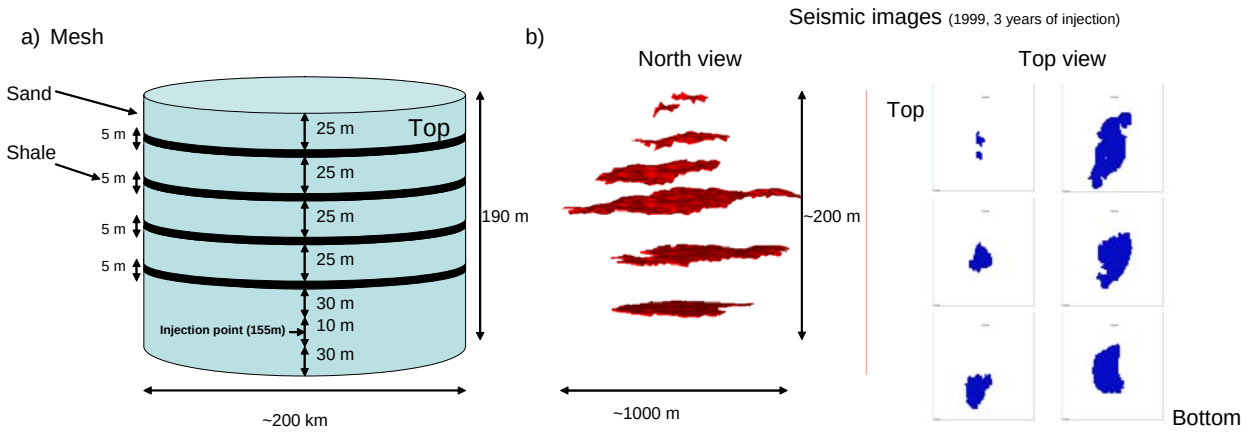

Fig. 6. a) Representation of the Utsira formation by a 2D multi-layered mesh with cylindrical symmetry. The CO_2 is injected in a cell at 160 m from the top of the formation. The porous media consist of highly permeable sands, separated by four semi-permeable shale layers. b) Vertical section and planar views of the seismic images three years after CO_2 injection (SACS, 2002; Arts and others, 2004)).

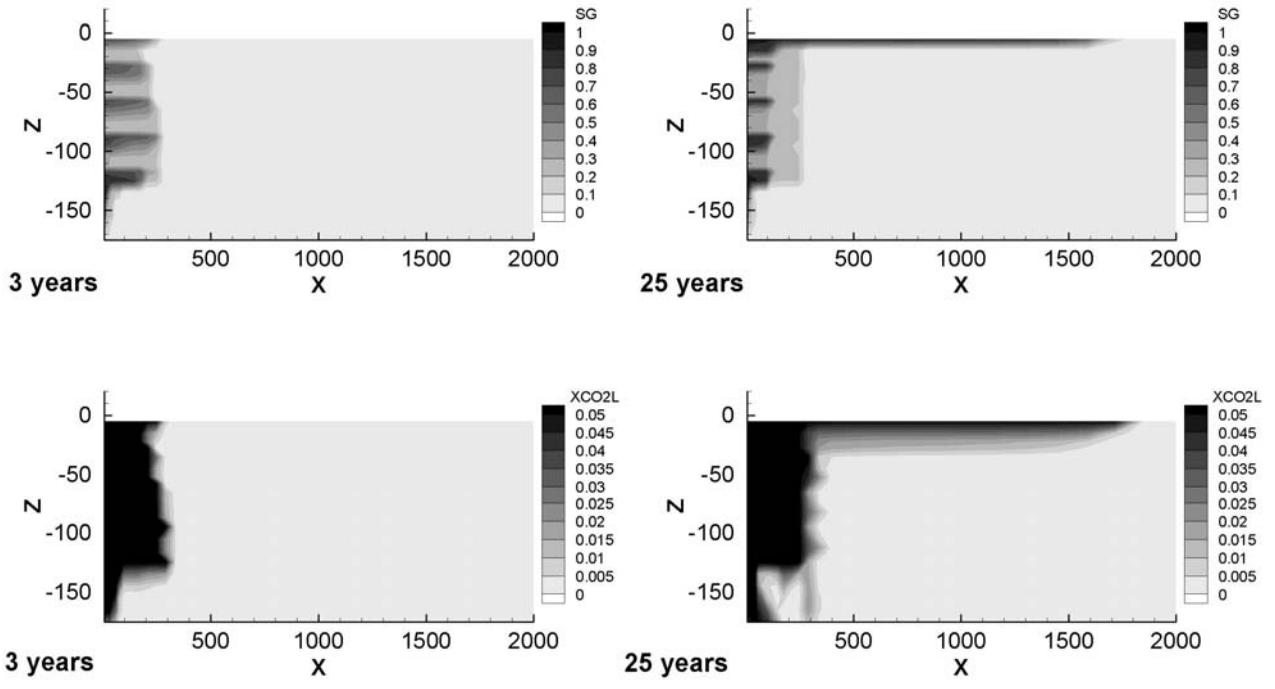

Fig. 7. Gas saturations (SG) and mass fractions of dissolved CO_2 in the liquid phase (XCO2L), after 3 years of injection and at the end of the injection period (25 years).

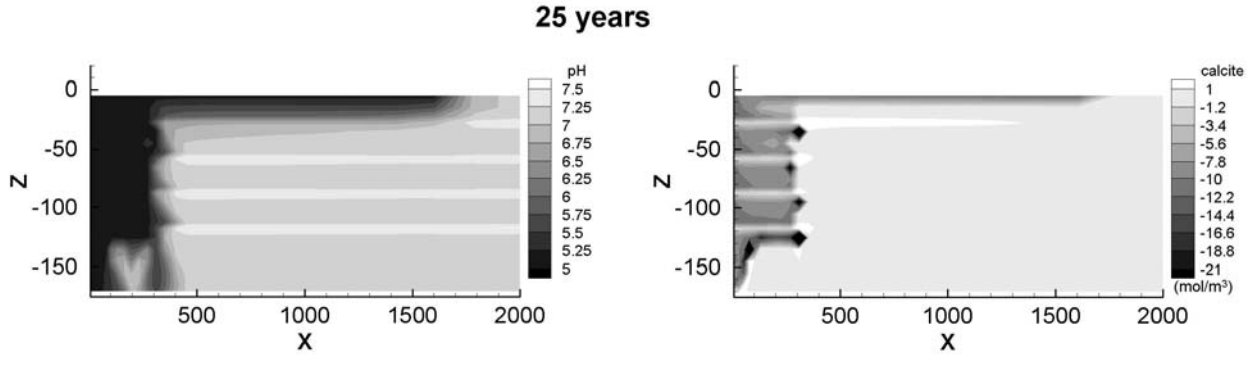

Fig. 8. pH and calcite dissolution at the end of 25 year CO_2 injection period. The negative sign corresponds to mineral dissolution.

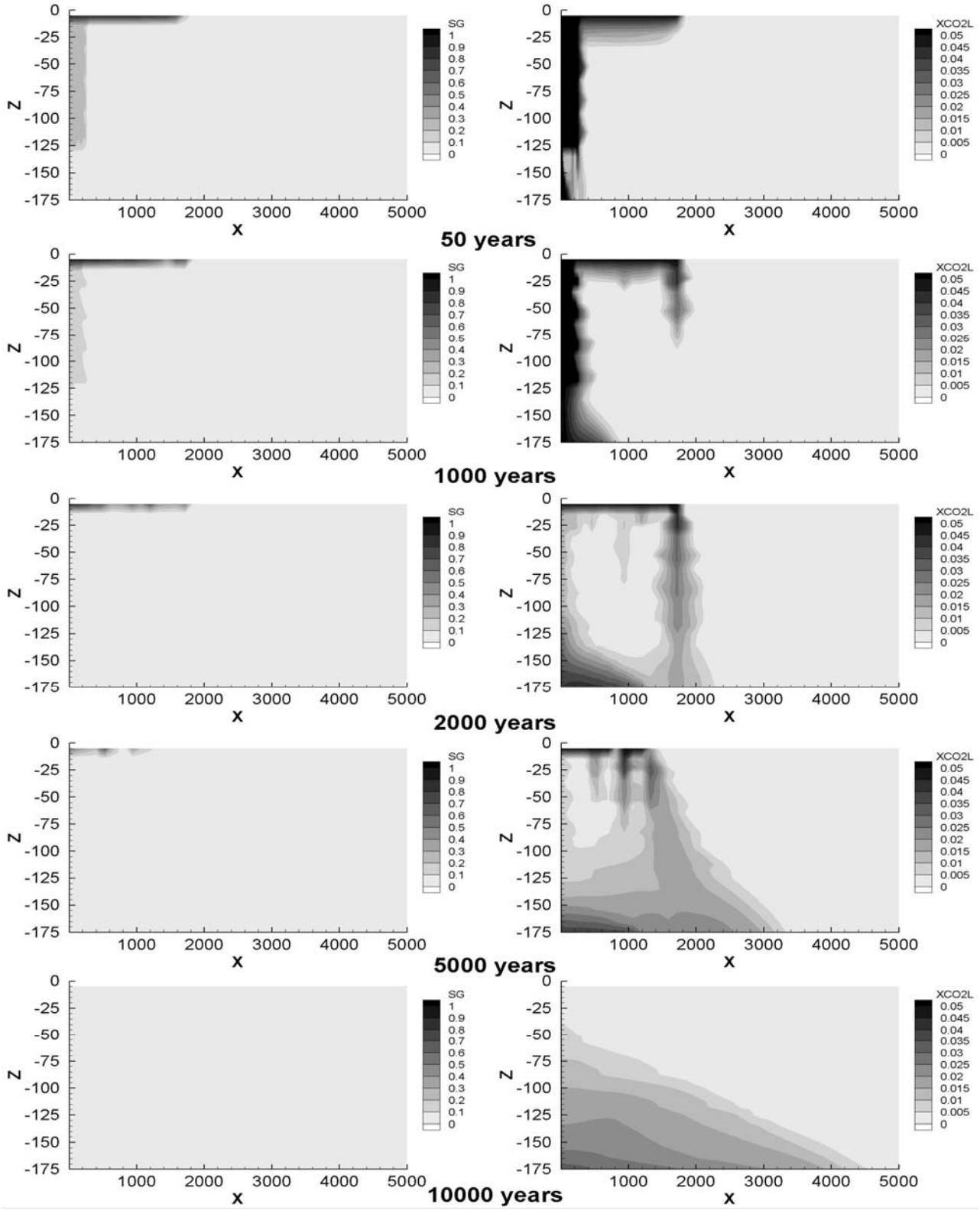

Fig. 9. Supercritical CO_2 gas phase (SG) migration and mass fraction of the dissolved CO_2 in the brine (XCO2L) simulated from 50 years after injection until 10,000 years.

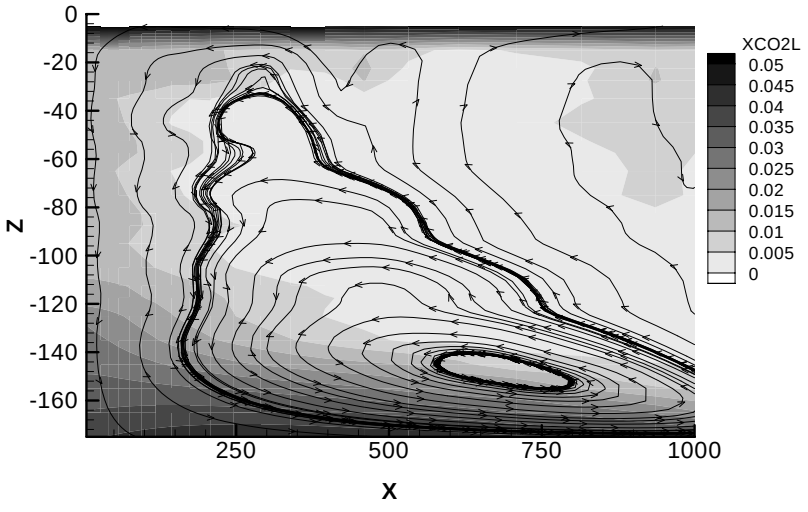

Fig. 10. Streamlines and dissolved CO_2 mass fractions XCO2L in the brine after 2,000 years. The streamlines highlight the convective fluid circulation induced by the mixing of brines containing dissolved CO_2.

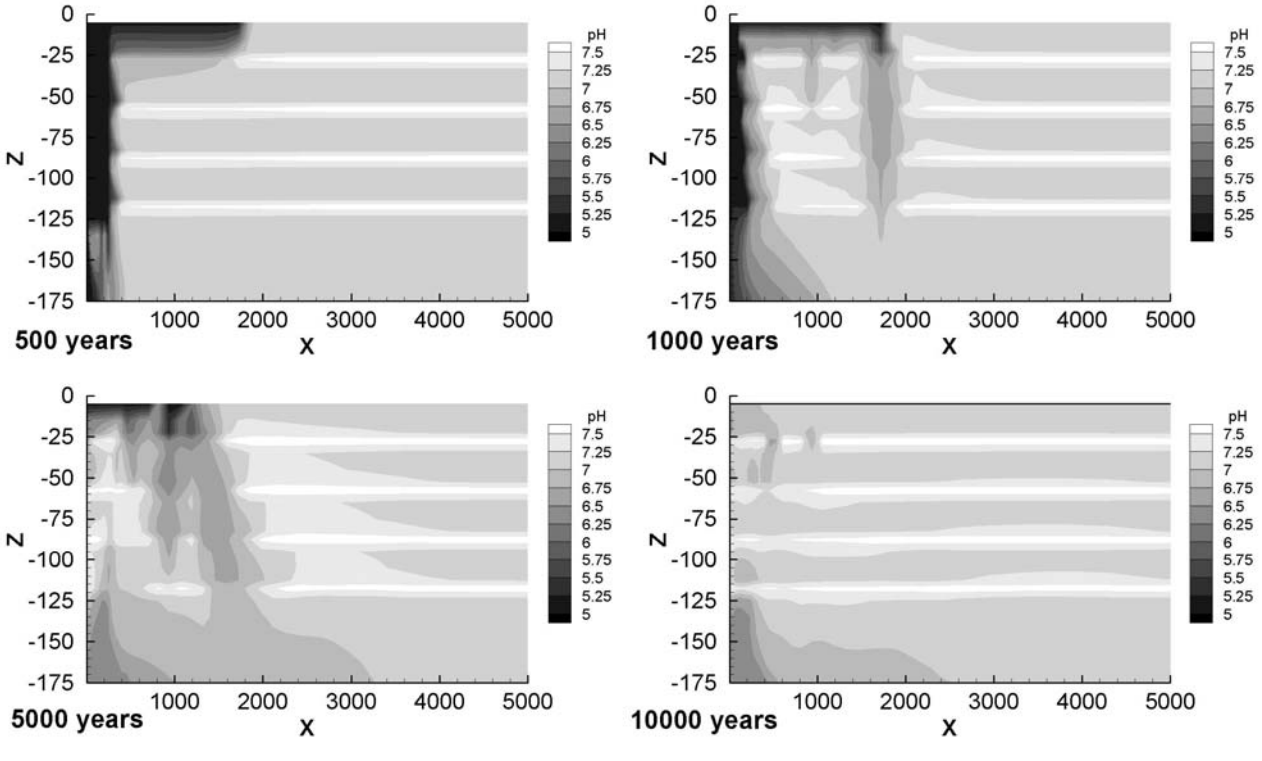

Fig. 11. pH evolution after 500, 1000, 5000 and 10 000 years, following 25 years of injection of

supercritical CO_2.

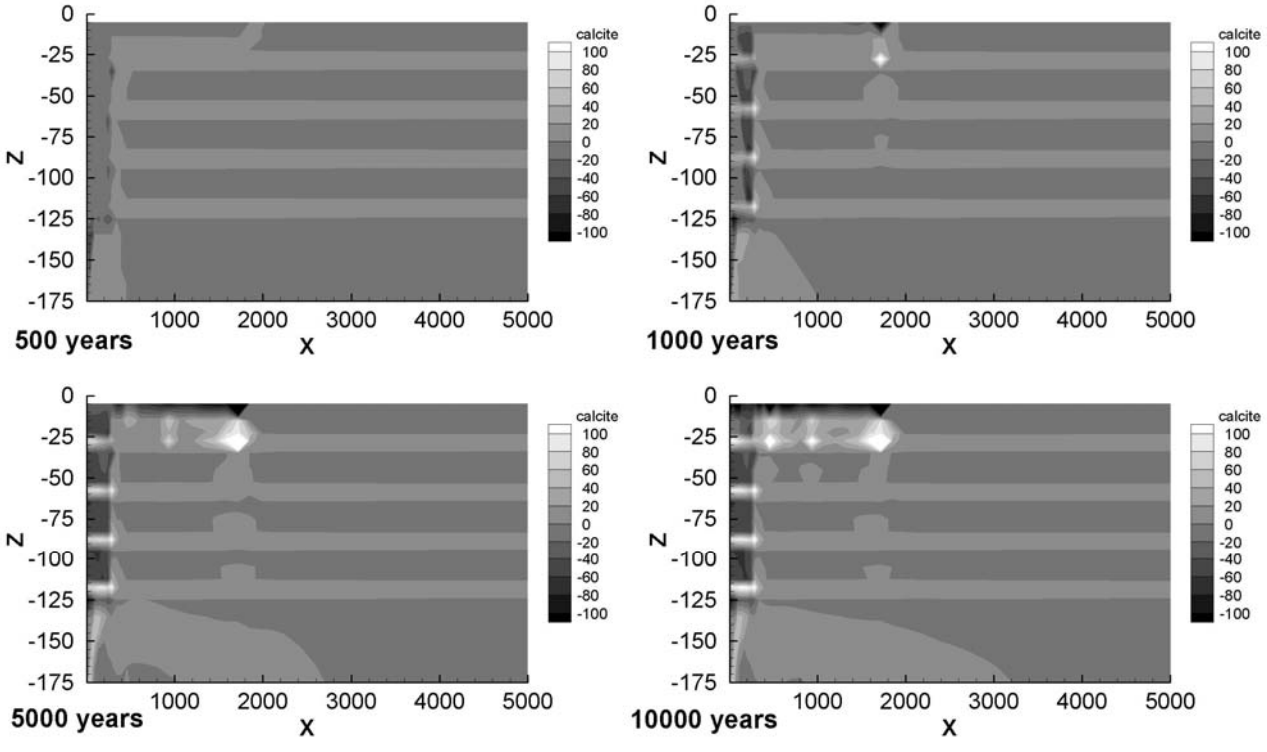

Fig. 12. Calcite mineral evolution in moles per m^3 of rock medium (negative sign for dissolution, positive sign for precipitation) after 500, 1000, 5000 and 10 000 years, following 25 years of injection of supercritical CO_2.

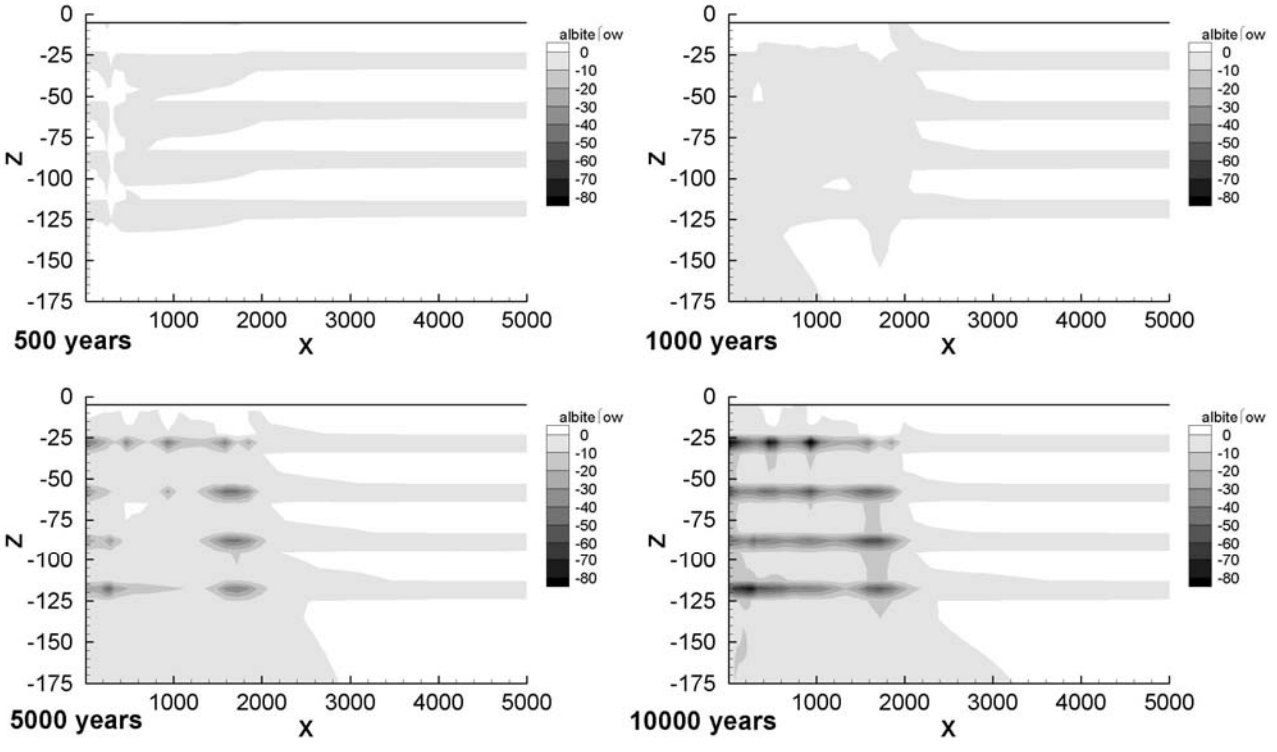

Fig. 13. Albite mineral evolution in moles per m^3 of rock medium (negative sign for dissolution, positive sign for precipitation) after 500, 1000, 5000 and 10 000 years, following 25 years of injection of supercritical CO_2.

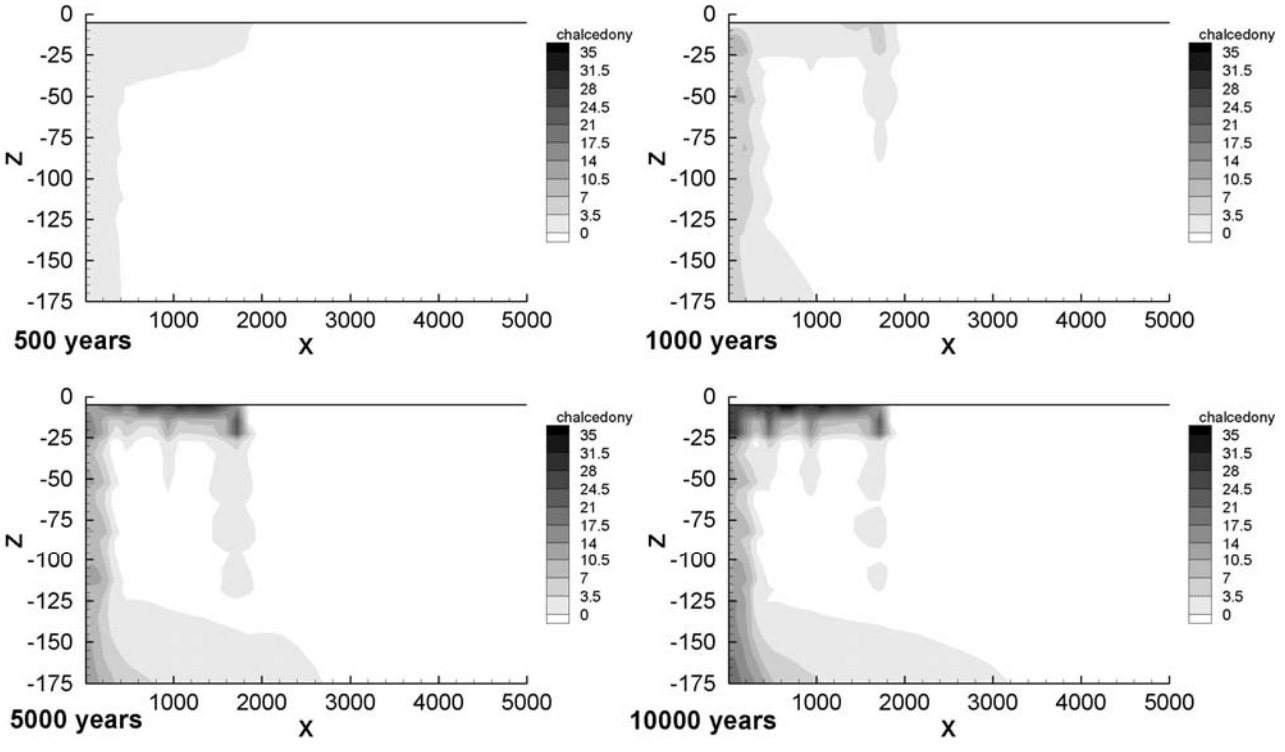

Fig. 14. Chalcedony mineral evolution in moles per m^3 of rock medium (negative sign for dissolution, positive sign for precipitation) after 500, 1000, 5000 and 10 000 years, following 25 years of injection of supercritical CO_2.

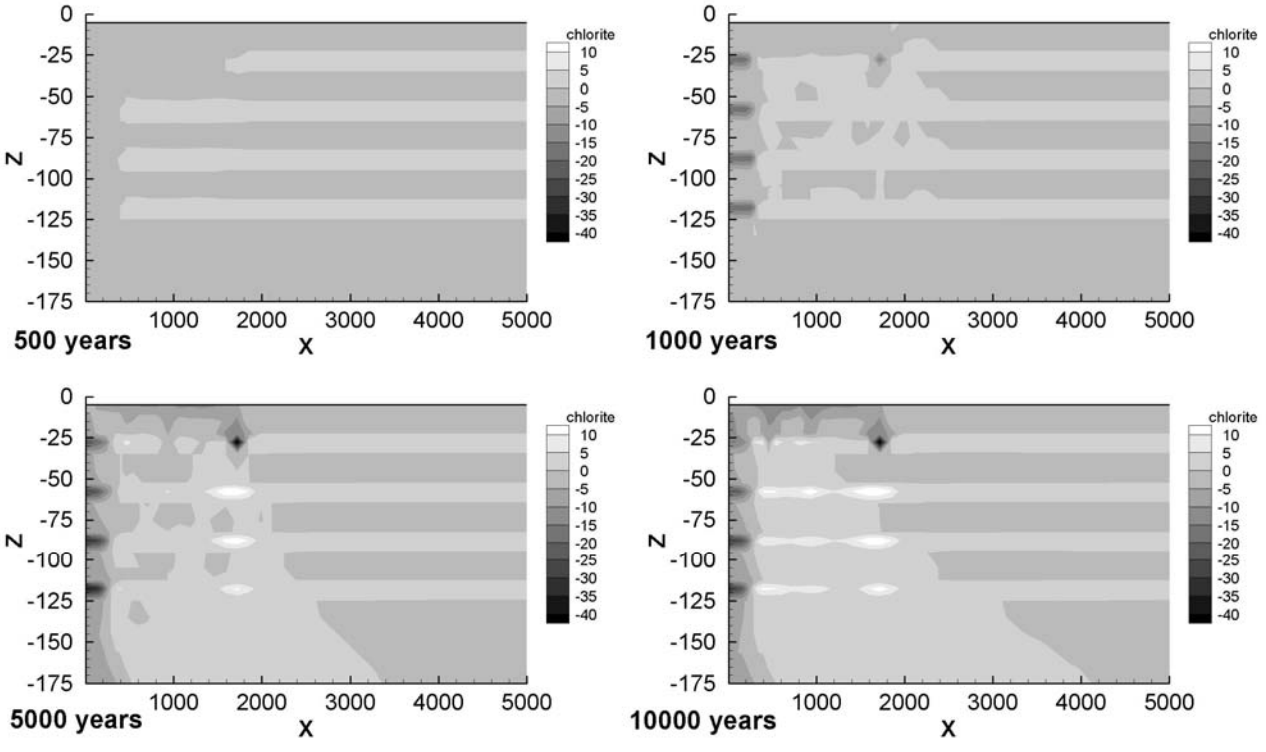

Fig. 15. Chlorite mineral evolution in moles per m^3 of rock medium (negative sign for dissolution, positive sign for precipitation) simulated after 500, 1000, 5000 and 10 000 years, following 25 years of injection of supercritical CO_2.

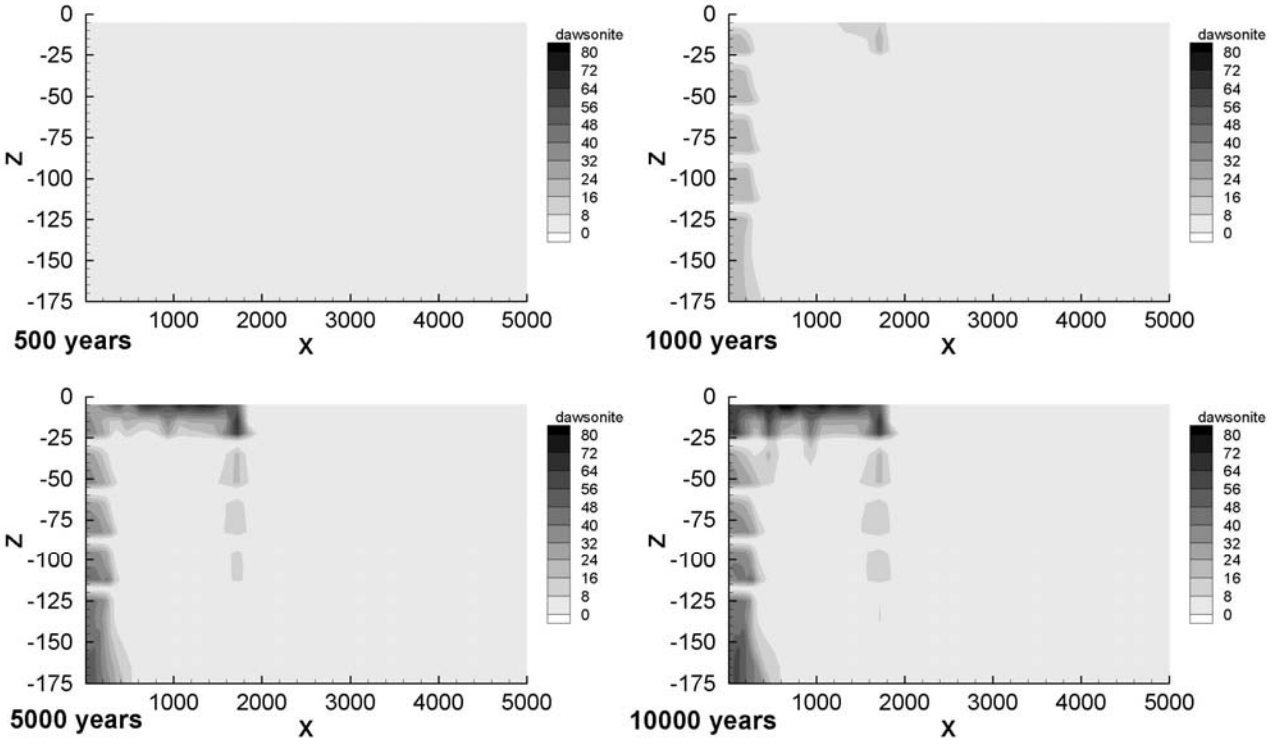

Fig. 16. Dawsonite mineral evolution in moles per m^3 of rock medium (negative sign for dissolution, positive sign for precipitation) after 500, 1000, 5000 and 10 000 years, following 25 years of injection of supercritical CO_2.

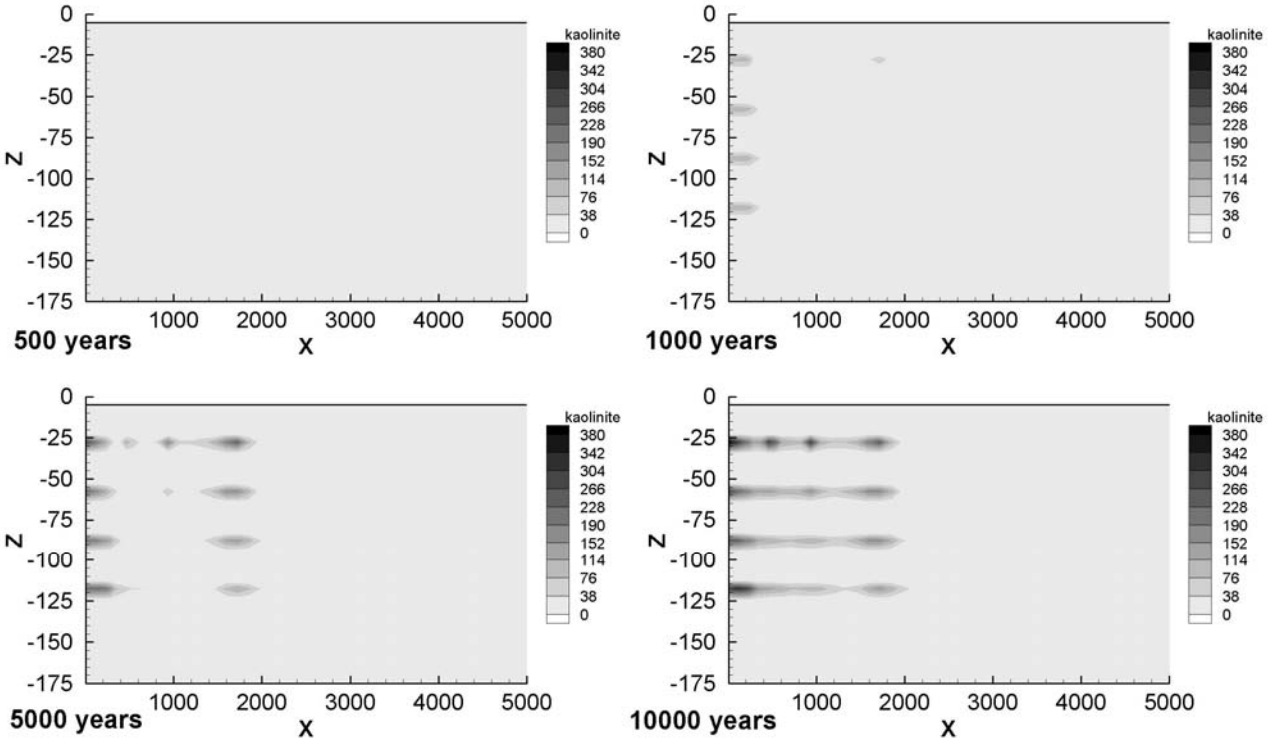

Fig. 17. Kaolinite mineral evolution in moles per m^3 of rock medium (negative sign for dissolution, positive sign for precipitation) after 500, 1000, 5000 and 10 000 years, following 25 years of injection of supercritical CO_2.

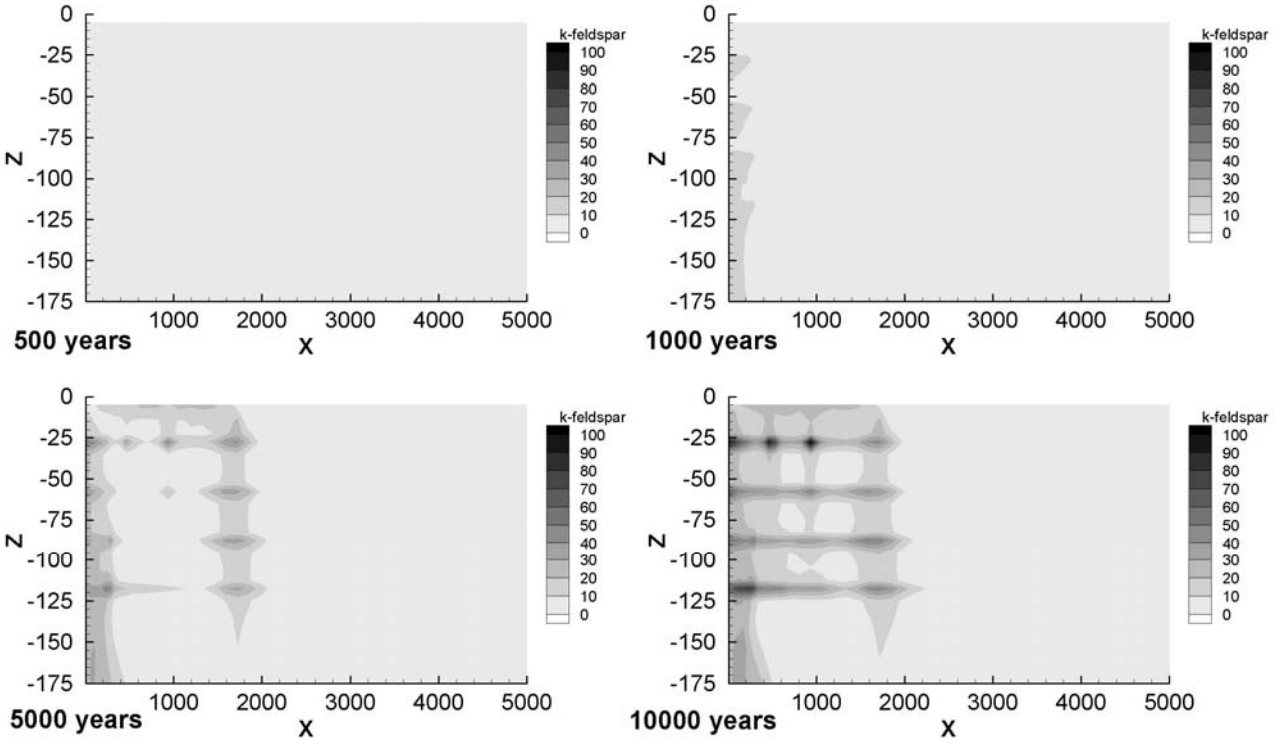

Fig. 18. K-feldspar mineral evolution in moles per m^3 of rock medium (negative sign for dissolution, positive sign for precipitation) after 500, 1000, 5000 and 10 000 years, following 25 years of injection of supercritical CO_2.

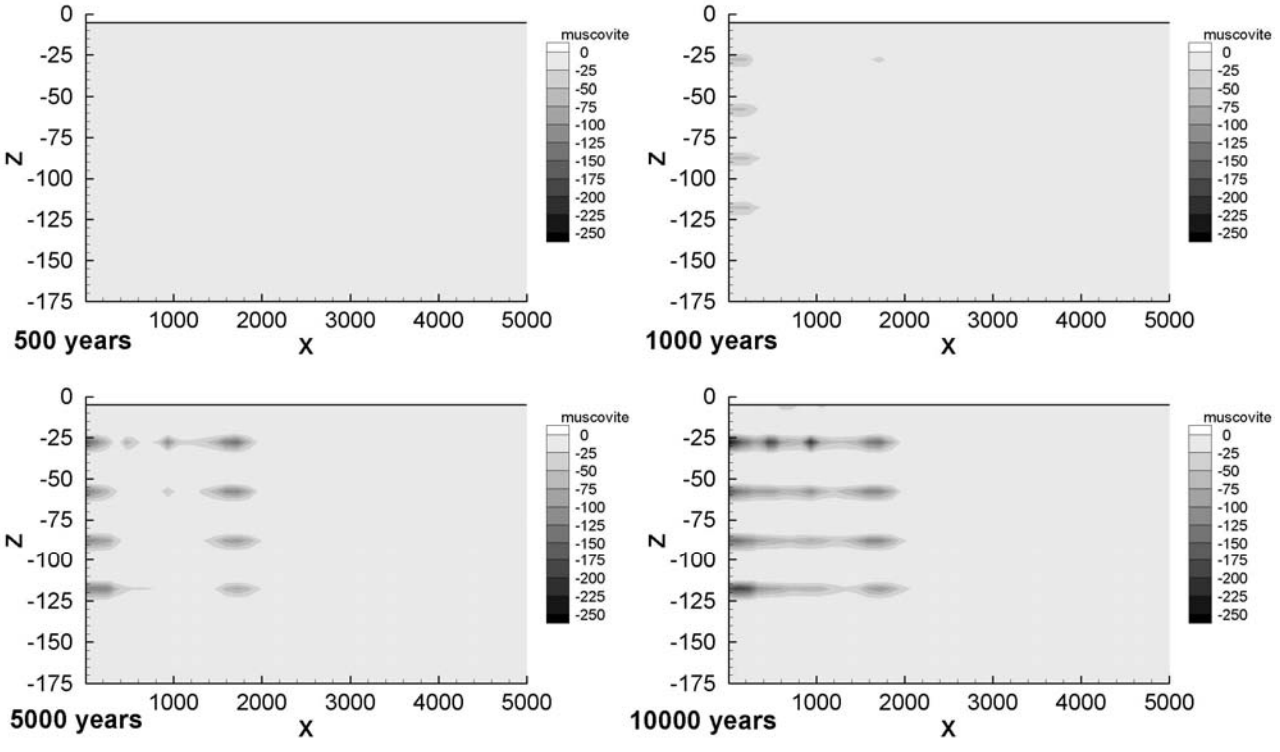

Fig. 19. Muscovite mineral evolution in moles per m^3 of rock medium (negative sign for dissolution, positive sign for precipitation) after 500, 1000, 5000 and 10 000 years, following 25 years of injection of supercritical CO_2.

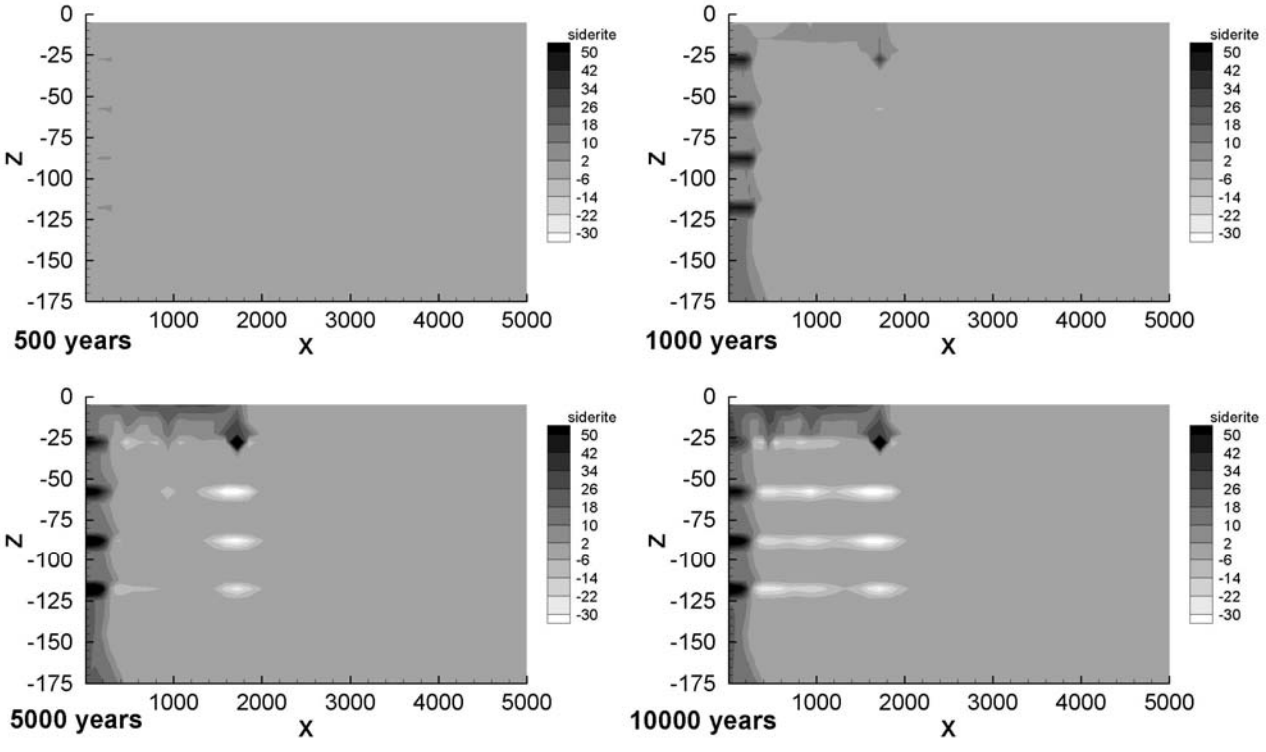

Fig. 20. Siderite mineral evolution in moles per m^3 of rock medium (negative sign for dissolution, positive sign for precipitation) after 500, 1000, 5000 and 10 000 years, following 25 years of injection of supercritical CO_2.

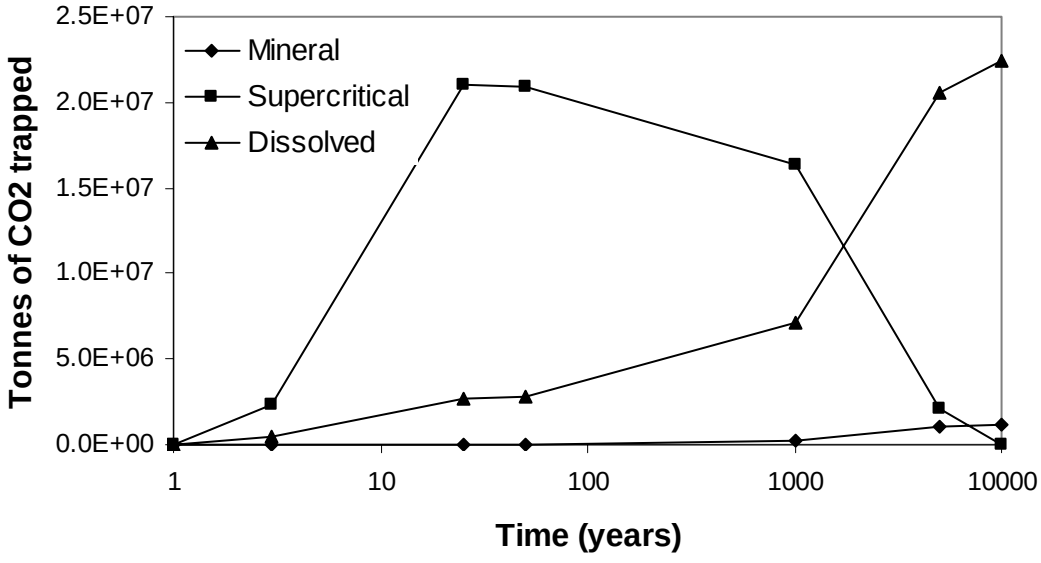

Fig. 21. Total amounts of carbon dioxide present as a free (supercritical) gas phase, dissolved in the aqueous phase, and sequestered in minerals.

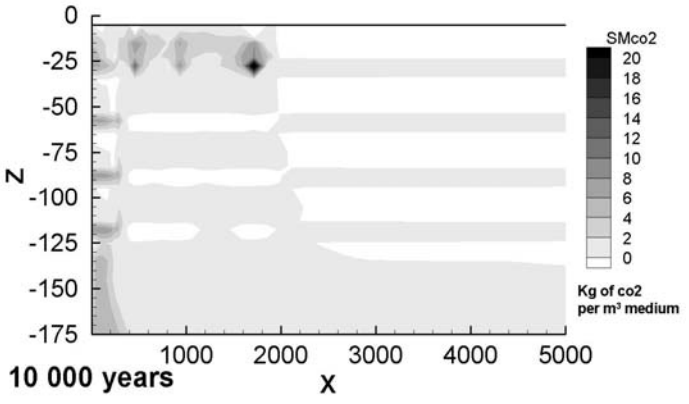

Fig. 22. Spatial distribution of the amount of carbon dioxide sequestered as minerals (SMco2), in kg of CO_2 per m^3 of rock.

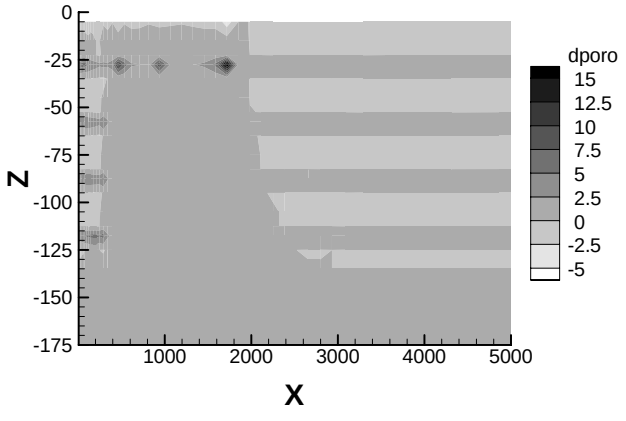

Fig. 23. Porosity changes after 10 000 years of simulation. dporo = 100 x $(\phi - \phi_{init})/\phi_{init}$. A porosity increase (dporo>0) of up to 15 % occurs in the shales, while a slight decrease (dporo<0) of less than 5 % is seen in the sands.

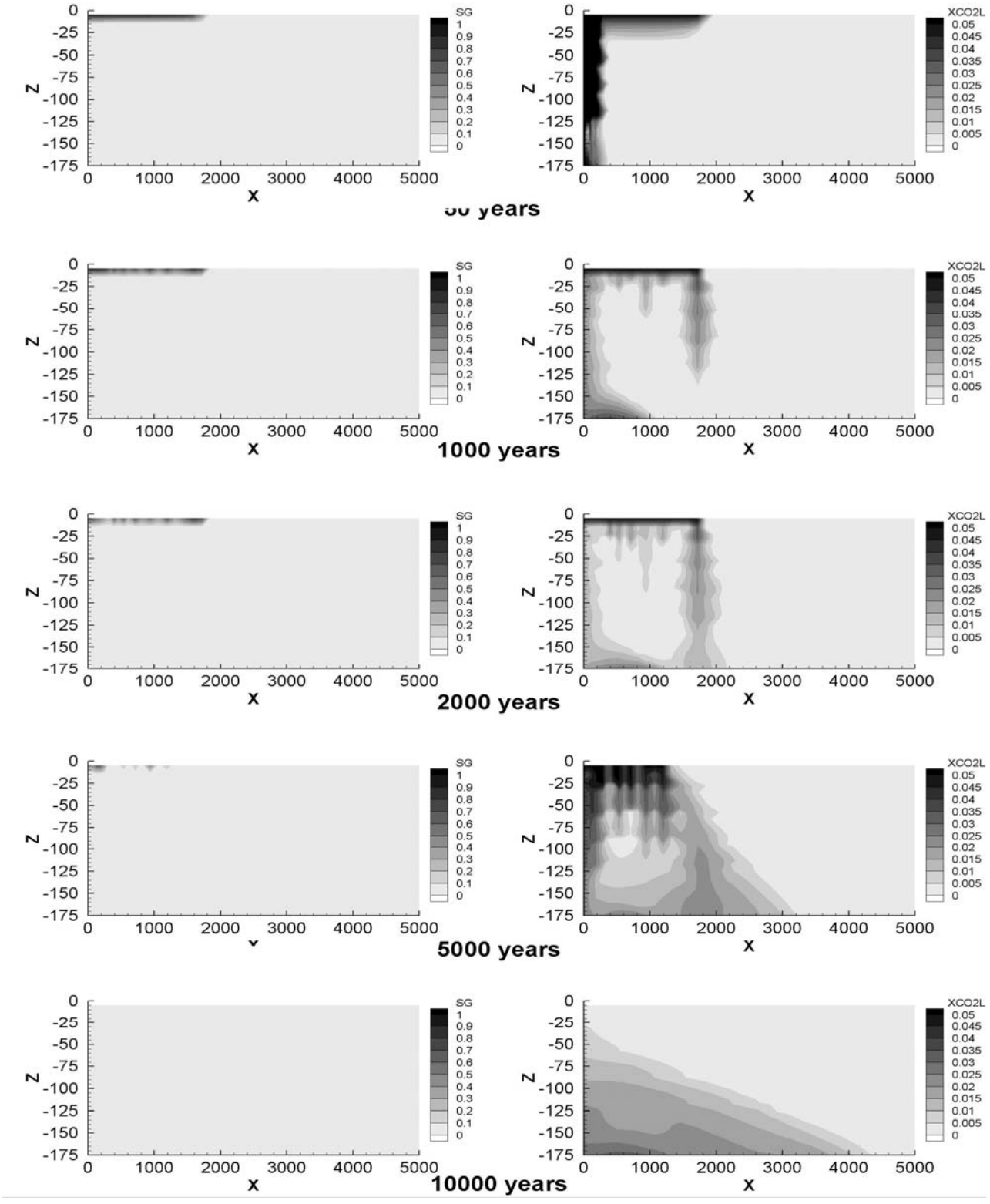

Fig. 24. Results obtained with residual gas saturation reduced to 0.05 (Case 2). Supercritical CO_2 gas bubble migration and mass fraction of the dissolved gas in the brine are shown for up to10 000 years,

following 25 years of injection of supercritical CO_2.

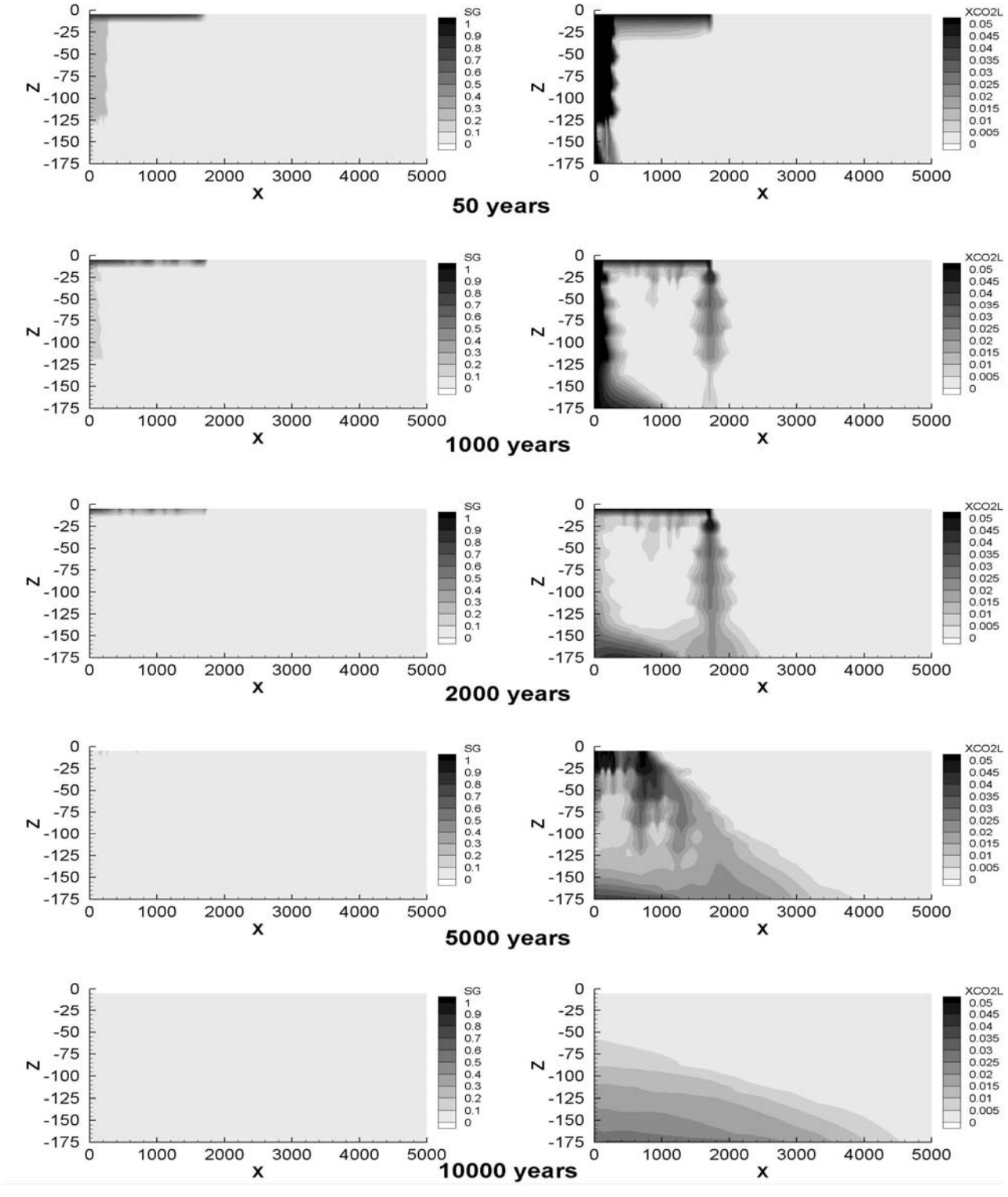

Fig. 25. Results obtained with the new mesh (case 3). Supercritical CO_2 gas bubble migration and mass fraction of the dissolved gas in the brine are shown for up to10 000 years, following 25 years of injection of supercritical CO_2.

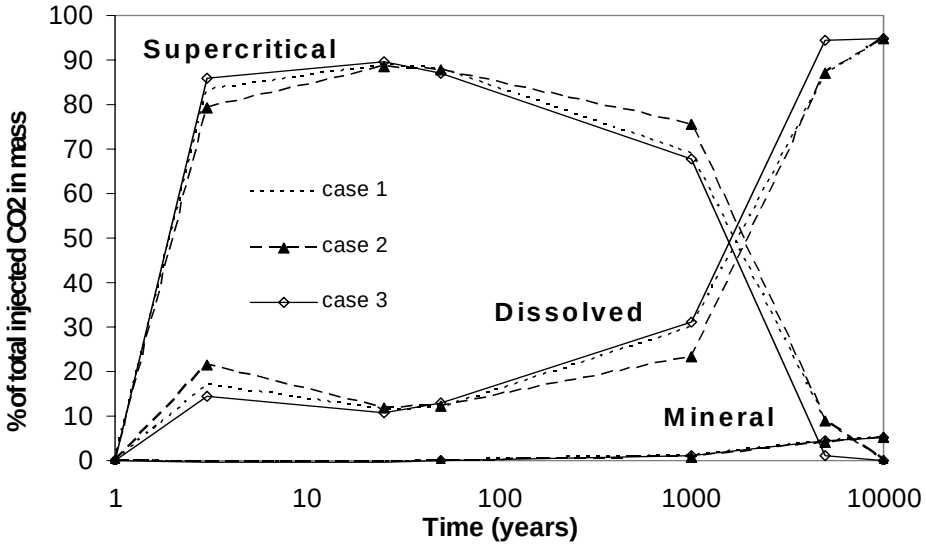

Fig. 26. Comparison of CO_2 inventories in the different phases for three different cases: Case 1 with the original mesh and a residual saturation of 0.20, Case 2 with the same mesh and a reduced residual gas saturation of 0.05, and Case 3 with a residual gas saturation of 0.20 and a mesh that is more refined near the injection point.